ESO

European Organisation
for Astronomical Research
in the Southern Hemisphere

Very Large Telescope

CUBES

Phase A study
Science Report

Doc. No.: VLT-TRE-ESO-13800-5679

Issue: 1

Date: 31.08.2012

Prepared: H. Kuntschner 31.08.2012
B. Barbuy
CUBES Science Team

Name Date Signature

Approved: F. Kerber
Name Date Signature

Released: L. Pasquini
Name Date Signature

CHANGE RECORD

ISSUE	DATE	SECTION/PARA. AFFECTED	REASON/INITIATION DOCUMENTS/REMARKS
1	31/08/12	All	First Release

TABLE OF CONTENTS

1 Scope 5
2 Abbreviations and Acronyms 5
3 Applicable and Reference Documents 6
3.1 Applicable Documents 6
3.2 Reference Documents 6
4 Executive Summary 7
4.1 The galactic science case 7
4.2 The extragalactic science case 8
5 Introduction 10
6 The galactic science case 11
6.1 Introduction 11
6.2 Heavy Elements in metal-poor stars 11
6.3 Carbon, nitrogen and oxygen abundances from molecular lines 14
6.4 Beryllium 17
6.4.1 Using solar twins to constrain Li and Be depletion 18
6.4.2 Mixing and stellar physics 19
6.4.3 Be as a cosmochronometer 19
6.4.4 Be and the formation of Globular Clusters 20
Target considerations 21
6.4.5 Spectral resolution and S/N requirements 21
6.4.6 Instrument requirements 26
6.5 Analysis of Planetary Nebulae in the UV 26
6.6 Novae, close binaries and compact stars 27
6.7 Bowen effect in Symbiotic stars, PN, AGN, and X-ray binaries 28
6.8 Surface gravity determination with hydrogen and helium lines 28
6.9 Interstellar matter 33
6.9.1 Major near-UV interstellar lines from the gaseous 33
6.9.2 Understanding the physical state of the multi-phase galactic interstellar medium and the processes at work 34
6.9.3 Near-UV lines and galactic ISM three-dimensional mapping 35
6.9.4 Diffuse interstellar bands 36
6.9.5 Circumstellar disks and planetary systems around white dwarfs 36
6.10 OH lines (308.5nm) as a tracer of Water in Comets 37
6.11 General spectral continuum integrity 39
7 The extragalactic science case 41
7.1 Introduction 41
7.2 Active Galactic Nuclei in the UV 41
7.2.1 The Narrow Line Region 42
7.2.2 The Broad Line Region 42
7.2.3 AGN circum-nuclear environment 43
7.2.4 Absorption systems 43
7.2.5 Instrument requirements 44
7.2.6 Target considerations 45
7.3 Quasar absorption line systems 48
7.3.1 The intergalactic medium at z = 1.5−2 48
7.3.1.1 Evolution of the IGM 48
7.3.1.2 The ionizing background at z=1.5−2 48
7.3.1.3 Metals in the IGM 49

7.3.1.4 Spatial structure 49
7.3.2 The galaxy-IGM interaction 49
7.3.3 The interstellar medium of high-*z* galaxies 50
7.3.4 Target considerations 51
7.3.5 Instrument requirements 51
8 Instrument competitiveness 53
8.1 Competition within ESO 53
8.2 World-Wide competition 53
8.2.1 Ground-based 53
8.2.2 Space-based: 54
8.3 Conclusion 54
9 Science Requirements 55
9.1 Observing modes 55
9.2 Wavelength range and spectral resolution 55
9.3 Required S/N ratios and exposure times 56
9.4 Pixel scale 57
9.5 Targets and field-of-view 57
9.6 Data reduction pipeline 57

1 Scope

This document presents the Science Report of CUBES (see also RD2). It contains a detailed description of the science cases considered during Phase A and establishes the hereby-derived science requirements.

The CUBES Science Report was prepared by the CUBES Instrument Scientist (Harald Kuntschner) and the PI of Phase A (Beatriz Barbuy) together with the members of the CUBES Science Team: Piercarlo Bonifacio (Observatoire de Paris, France), Marcos Diaz (IAG, Brazil), Roger Ferlet (IAP, France), Paul Groot (University of Nijmegen, Netherlands), Patrick Petitjean (IAP, France), Thomas Rauch (University of Tübingen, Germany) and Eline Tolstoy (University of Groningen, Netherlands). Science cases or contributions to them were kindly provided by Olivier Hainaut, Rosine Lallement and Giovanni La Mura. For specific questions support was kindly provided by ESO employees. For example, Rodolfo Smiljanic performed simulations to further explore the required S/N and spectral resolution requirements of the Be case (see Section 6.4.5).

2 Abbreviations and Acronyms

This document employs several abbreviations and acronyms to refer concisely to an item, after it has been introduced. The following list is aimed to help the reader in recalling the extended meaning of each short expression:

AGN	Active galactic nuclei
CUBES	Cassegrain U-band Brazilian-ESO Spectrograph
E-ELT	European Extremely Large Telescope
ESO	European Southern Observatory
ESPRESSO	Echelle Spectrograph for Rocky Explanet and Stable Spectroscopy Observations
HST	Hubble Space Telescope
IGM	Inter galactic material
ISM	Inter stellar material
UV	Ultra violet
UVES	UV-Visual Echelle Spectrograph
VLT	Very Large Telescope

3 Applicable and Reference Documents

3.1 Applicable Documents

The following Applicable Documents (AD) of the exact issue form part of the present document to the extent specified herein.

AD Nr	Doc Nr	Doc Title	Issue	Date

3.2 Reference Documents

The following Reference Documents (RD) contain useful information relevant to the subject of the present document.

RD Nr	Doc Nr	Doc Title	Issue	Date
RD1	STC-501	Science opportunities arising from a high-throughput UV spectrograph at the VLT	1	28.03.2012
RD2	VLT-SOW-ESO-13800-5639	CUBES Phase A Study – Statement of Work	1	18.07.2012

4 Executive Summary

A high-efficiency, medium-resolution (R ~ 20,000 - 25,000) spectrograph dedicated to the UV (here defined as 300 - 400 nm) offers a wealth of new and relevant information for galactic as well as extragalactic astronomy. With modern instrument designs, high efficiency dispersing elements and UV-sensitive detectors, the predicted gain in sensitivity over UVES, the main VLT work horse at this spectral resolution, corresponds to about 2 magnitudes at 350 nm, and up to 3 magnitudes at 320 nm, enabling vastly increased sample sizes accessible to the astronomical community. For example, CUBES will be able to achieve in only 45 min exposure time a S/N of greater than 50 per detector pixel for a point source of V=16 and λ > 320nm. Due to the focus on near-IR spectroscopic instrumentation foreseen at all major observatories (including the E-ELT) CUBES will remain a unique capability of the VLT for many years to come. Interesting cooperative opportunities arise from spectrographs with complementary wavelength coverage, such as ESPRESSO at the VLT or the spectrographs on the World Space Observatory-Ultraviolet.

While the proposed spectral range (UV 300 – 400 nm) and spectral resolution (R ~ 20,000) have been available at large telescopes before, the combination of maximized spectrograph efficiency and high enough spectral resolution to study individual lines in stars as well as detailed velocity structures in galaxies, will enable access to sizable (and therefore statistically meaningful) target samples, 2−3 magnitudes deeper than UVES, in key astrophysical areas for the first time.

4.1 The galactic science case

The galactic science case is dominated by stellar abundance studies but also offers exiting opportunities for the observation of e.g. comets or the ISM. The UV spectra of stars contain a high density of key absorption lines including many elements that are unique to this spectral range (e.g. Bi I 302.4nm, U II 385.9nm), particularly important for the study of old metal-poor stars. Because of their long lifetimes, low-mass metal-poor stars retain in their atmospheres a fossil record of the chemical elements in the interstellar medium at the time of their formation. Their abundances thus enable near-field cosmological studies that are considered one of the top ten scientific results of ESO.

Recent and ongoing surveys (e.g. HK/HES, SDSS-II SEGUE, RAVE) are efficiently finding new, very metal-poor stars, in the regime of $V \simeq 16$ or fainter, and more will come with GAIA. These stars, which are likely to be among the oldest stars in the Galaxy, are primary targets for an efficient UV spectrograph and not realistically accessible to UVES below ~380 nm due to lack of throughput. The SDSS-DR8 survey and HK/HES alone provide ~10,000 potential metal-poor ([Fe/H] <−2.0, V<17) targets observable from the VLT. In the following we list selected examples for the proposed stellar science:

- Surprisingly, the site of production for r-process elements is still unknown. The wealth of absorption lines in the UV allows the study of heavy elements in metal-poor stars, in order to better understand the r-process itself, and to have constraints on the nature of the first stars (Population III).
- Several carbon, nitrogen and oxygen molecular bands are available in the UV range and are crucial to the study of the chemical evolution of the Galaxy. For example, the near-UV OH lines are the only ones strong enough to determine the oxygen abundance in metal-poor turn-off dwarf stars. The strong NH bandhead at 336 nm can be used to derive nitrogen abundances directly, as compared to the indirect determinations via CN bands.
- Perhaps most importantly, the UV is our only spectral window for the determination of the Beryllium abundance with the Be II resonance lines at 313.042 and 313.107 nm. ^{9}Be behaves as a primary element and is a pure product of Galaxy-wide cosmic-ray spallation

of heavy (mostly CNO) nuclei in the interstellar medium. Therefore, its abundance shows a good correlation with time and can be employed as an independent cosmochronometer for the early stages of the Galactic evolution (halo stars, globular cluster stars etc.). Since Be cannot be produced through stellar evolution it is also a very useful baseline for the detailed study of light element production in Globular Clusters (GC), which offer unique insights into the detailed star-formation processes, and in some cases for several star generations in GCs.

In order to allow for clear line separation, all of the above stellar science cases require a minimum spectral resolution of R ~ 20,000. Therefore, these science cases are not suitable for X-shooter UVB arm spectroscopy (R ~ 6,000).

4.2 The extragalactic science case

The extragalactic science case identified two primary fields of interest for CUBES: (1) investigations of active galactic nuclei (AGN) and (2) studies of the inter-galactic medium (IGM). In the following we outline three examples for the proposed science:

- Nearby AGN represent a naturally attractive target since their characteristic features, including an intense continuum of ionizing radiation rising towards the UV, as well as several emission lines (e.g. [Ne V]342.6nm, [O II]372.7nm, [Ne III]386.8nm) that originate from an extremely compact source, reveal much more physical detail, concerning their nature, than any current imaging technique can achieve. The near-UV spectral window, in particular, is a precious wavelength range for addressing fundamental questions, ranging from the physics of nuclear activity itself, to the influence of AGN on the properties of their host galaxies and on cosmological evolution. Although the profiles of broad and narrow emission lines are commonly exploited to investigate the dynamical influence of the AGN central engines at various distance scales, a spectral resolution of R ~ 20,000 is needed to explore the kinematical components of the line emitting plasma and to address the problem of its ionization source. The UV contains emission lines covering a wide range of ionization conditions and hence represents an ideal wavelength range for this investigation. Up-to-date AGN catalogues list more than 1300 AGN targets with V<16 observable from the VLT and the numbers rise steeply for fainter targets. Therefore, a high-efficiency UV spectrograph will be able, for the first time, to probe large samples of objects whose characteristics are extremely rare or perhaps totally missing in current, brighter magnitude-limited samples.
- Observing AGN at increasing redshifts enables the study of emission lines at bluer rest-wavelengths. CUBES will allow us to close the gap between the space-based (e.g. HST/COS and STIS with typically λ≤300 nm) and optical to red (400−900 nm) ground-based efforts in this field. Broad emission and absorption lines constrain the structure of the central engine and the dynamics of its accretion flows. The provision of highly efficient, medium-resolution spectroscopy in the UV allow to probe a closer redshift range than is currently accessible. Several hundreds of targets could be investigated to test AGN properties against selection effects (rather than being limited to the study of only the brightest AGN) and to study cosmological evolution.
- The UV is of utmost importance for the study of (i) the IGM at intermediate redshifts (z≃1.5−2), its physical state (temperature, ionization) but also its metal content (through O VI), and (ii) the interstellar medium of high redshift galaxies and in particular its molecular content (H_2 for z>2; CO for z>1 given CUBES wavelength range). Medium spectral resolution is needed to decompose the absorption profiles and also to derive accurate characteristics of the absorption lines (column density and Doppler parameter).

A spectral resolution of R ~ 20,000 associated with very high efficiency below 400 nm is a good compromise between this necessity and the need to target fainter quasars. No currently available spectrographs including VLT/UVES offer this balance. The SDSS-BOSS project will provide more than 50,000 QSOs at z>2 and accessible from the VLT thus providing a rich target database for CUBES.

5 Introduction

This document presents a collection of science cases for the Phase A study of CUBES (see RD1, RD2). CUBES is a high efficiency, medium-resolution (R ~ 20,000 - 22,000 at 320 nm) spectrograph dedicated to the UV (here defined as 300−400 nm). Such an instrument offers a wealth of new and relevant information for stellar as well as extragalactic astronomy. Although the atmosphere presents a natural cut-off at about 300 nm (see Figure 1), with modern instrument designs, high-efficiency dispersing elements and UV-sensitive detectors, the predicted gain in sensitivity over UVES, the main VLT work horse at this spectral resolution and wavelength range, corresponds to about 2 magnitudes at 350 nm, and up to 3 magnitudes at 320 nm, offering vastly increased sample sizes accessible to the astronomical community. For example, CUBES will be able to achieve in only 45 min exposure time a S/N of greater than 50 for *V*=16 and λ > 320nm.

Two main scientific areas have been explored: (i) a collection of stellar science and other galactic cases presented in Section 6 and (ii) extragalactic themes discussed in Section 7. Beyond these specific science goals we stress the potential of general use to the ESO user community by offering a high-efficiency spectrograph in this understudied wavelength range. We briefly discuss the general competitiveness of such a spectrograph with respect to existing or planned facilities in Section 8 and provide a summary of the science requirements in Section 9.

To aid the development of the science case a preliminary ETC was setup. This ETC contains information about the estimated throughput of the main components but does not yet take into account the currently foreseen slicer design for the entrance slit. The ETC can be found at: http://www.eso.org/observing/etc/bin/gen/form?INS.MODE=swspectr+INS.NAME=cubes

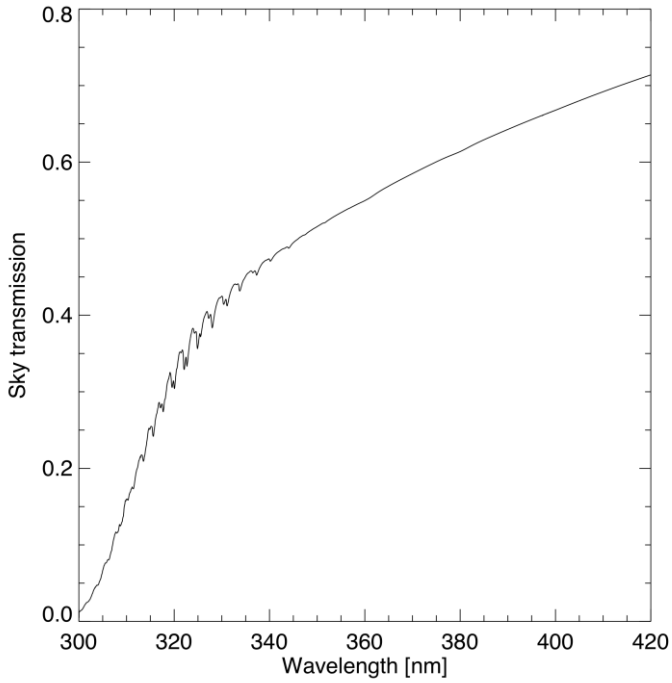

Figure 1: Predicted UV sky transmission on Paranal for an airmass of 1.3. Source: ESO Advanced Sky model SM-01 (June 18, 2012)

6 The galactic science case

6.1 Introduction

A high-efficiency, medium resolution spectrograph in the UV (300−400 nm) would bring a wealth of new information on several topics in galactic astronomy. The emphasis is put on stellar science but other topics are explored as well. The UV contains the highest density of stellar lines, and includes lines of many elements that are not found elsewhere. Furthermore, this wavelength range is especially important for the study of old metal-poor stars (Sections 6.2 & 6.3). Because of their long lifetimes, low-mass metal-poor stars retain in their atmospheres a fossil record of the chemical elements in the interstellar medium at the time of their formation. This enables near-field cosmology studies.

In particular, the study of Beryllium (Section 6.4), heavy elements, and C, N, O molecular bands in metal-poor old stars is of great interest. For $V \leq 17$ there are thousands of targets available from the SDSS and HK/HES surveys: 9849 stars with [Fe/H] <−2.0 in the SDSS-DR8 survey, 6485 of them reachable from VLT. For the HK/HES surveys there are 4366 such stars, with 3522 reachable from the VLT. The predicted gain in sensitivity for this spectrograph over UVES, the main VLT player at this spectral resolution and wavelength, corresponds to about 2 magnitudes at 350 nm, and up to 3 magnitudes at 320 nm. For example, it will be possible to achieve in only 45 min exposure time a S/N of ~50 per spectral bin at 350 nm for V = 16 (G0V template, airmass=1.3, slit-transmission factor = 0.83).

Studies of planetary nebulae (Section 6.5), novae (Section 6.6), symbiotic stars (Section 6.7), the ISM (Section 6.9), and even comets (Section 6.10) would also greatly benefit from diagnostics available in UV spectra. The noteworthy aspect of spectral continuum integrity resulting from using a classic longslit design without cross dispersion is outlined in Section 6.11.

6.2 Heavy Elements in metal-poor stars

The site of production of r-elements is still not known (e.g. Kratz et al. 2007; Thielemann et al. 2010). This problem has been identified as being among the greatest challenges in physics, by Science Magazine. The presently preferred model involves neutrino winds, in which free nucleons are bombarded by a neutrino-driven wind of neutron-rich matter near the neutrino sphere of a core-collapse supernova (Arnould et al. 2007 and references therein). Neutron star mergers, and neutron star formation during accretion-induced collapse are the other main candidate models to be tested.

The best way to help with this situation is the observation of the results of the ’r’ process in various circumstances. The abundances of the elements and isotopes produced by this process are known in some detail in the solar system. It is therefore important to try to find similar information in a very different environment: the first phases of the evolution of our Galaxy. For this it is necessary to derive abundances of heavy elements in the first (38<Z<48), second (56<Z<72) that involve the so-called rare earth elements, and third peaks (76<Z<88), and the actinides (Z>89). Many of the neutron-capture heavy elements have dominant transitions in the near-UV and some can *only* be measured in the near-UV and/or UV.

In the wavelength region 300−400 nm there are many rather strong lines of Y II, Zr II, Nb II, Pd I, Ag I, La II, Ce II, Nd II, Eu II, Gd II, Tb II, Dy II, Ho II, Er II, Tm II, Os I, Ir I, Pb I, Th II (see Cowan et al. 2005). A few elements only have lines near to the lower limit of this region: Bi I 302.4 and 306.7nm, whereas near to the upper limit there are lines of the unique measurable line of uranium at U II 385.9, Pr II 396.4, Sm II 389.6, and well-defined strong lines such as Ba II 389.1 and Eu II 393, 397.1 nm.

Therefore, the study of heavy elements in metal-poor stars, in order to better understand the r-process itself, and to have constraints on the nature of the first (Population III) stars, is one of the main topics that could be addressed with the proposed spectrograph.

Spectral resolution considerations for the determination of heavy elements:

Given the desire to reach faint targets, a priori it is not clear which spectral resolution is the most suitable one for this kind of studies. Perhaps most notably, HST/STIS studies in the UV worked successfully with R~30,000. For the proposed ground-based spectrograph it is of paramount importance to maximize throughput and by implication determine the minimum suitable spectral resolution. The discussion can be focused on the study of the following lines:

- UII 385.957nm, unique measurable line of uranium a radioactive element that, if detectable, gives directly the stellar age;
- BiI 302.4635nm, unique measurable line of Bismuth (given that the BiI 306.7nm line is severely blended), that can be important as a reference element, which together with uranium, can be used to derive stellar ages;
- GeI 303.907nm: Germanium can serve as a key element to constrain physical conditions for the r-process nucleosynthesis.

These 3 lines were investigated as follows:

The **UII 385.9nm** line was computed for 4 resolutions, from 20,000 to 30,000, and compared with the line for the uranium-rich star CS 31082-001 observed with UVES. The synthetic spectrum computed with its final value (as shown in Cayrel et al. 2001, Nature, 409, 691), indicate that this faint line is far too smoothed by the lower resolution, and at least R~30,000 is needed. We suggest not to select this line and proceed as follows: if a metal-poor star shows other r-process enhancements, then it is worth applying to detect UII 385.9nm with e.g. UVES or ESPRESSO.

BiI 302.4635nm: In Figure 2 we show the BiI 302.4635nm line observed with HST/STIS (R~30,000; see Barbuy et al. 2011), compared with calculations at R=30,000. This line is rather well defined and not blended, and thus would be confidently observable at R~20,000.

GeI 303.97nm: Figure 3 shows the GeI 303.97nm line computed with resolutions of 18,000 up to 25,000, compared with a HST/STIS spectrum (Siqueira Mello Jr et al. 2012, submitted). It is clear that this line is suitably measurable at a resolution of R>18,000.

For many other equally important atomic lines of heavy elements we confirmed that a spectral resolution of R~20,000 is sufficient. Lines include: AgI 328.07nm, AgI 346.47nm, LuI 307.76nm, MoI 366.41nm, ReII 330.22nm, ReII 358.012nm, RuII 349.894nm, RuII 379.89nm, TaII 313.74nm. Closer to 400nm there are very good lines of Europium EuII 372.406nm, EuII 393.05nm, EuII 397.197nm.

Typical S/N ratios needed for the study of heavy elements are at least S/N ~ 50. Conclusions on the instrument requirements are given in Section 6.4.6 together with the results form the Be line.

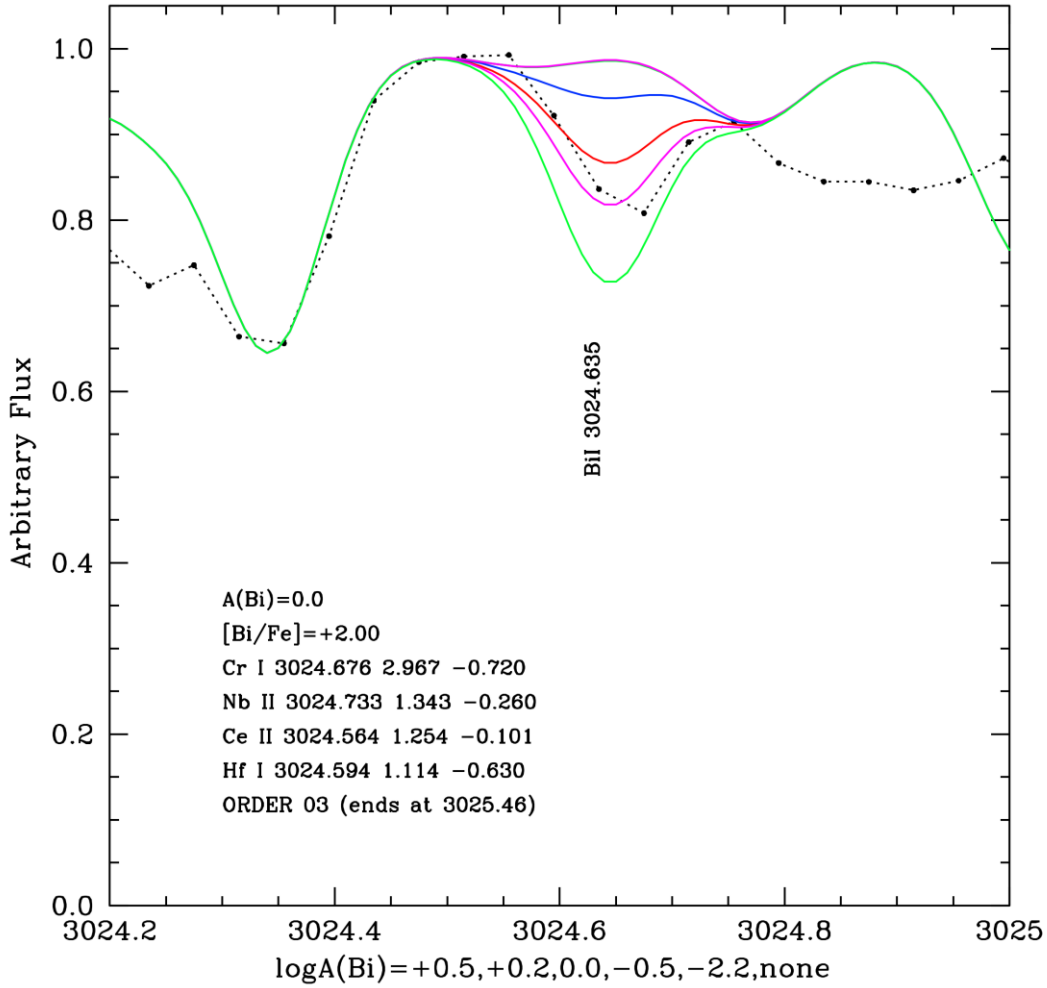

Figure 2: BiI λ302.46nm line observed with HST/STIS (star: CS 31082-001; black dotted line) compared with synthetic spectra computed with abundances A(Bi) = +0.5, +0.2, 0.0, -0.5, -2.2, and no Bi, at a resolution of R~30,000 (colored lines; Barbuy et al. 2011). The line is clearly detectable and not blended, therefore also detectable at a lower spectral resolution of R~20,000.

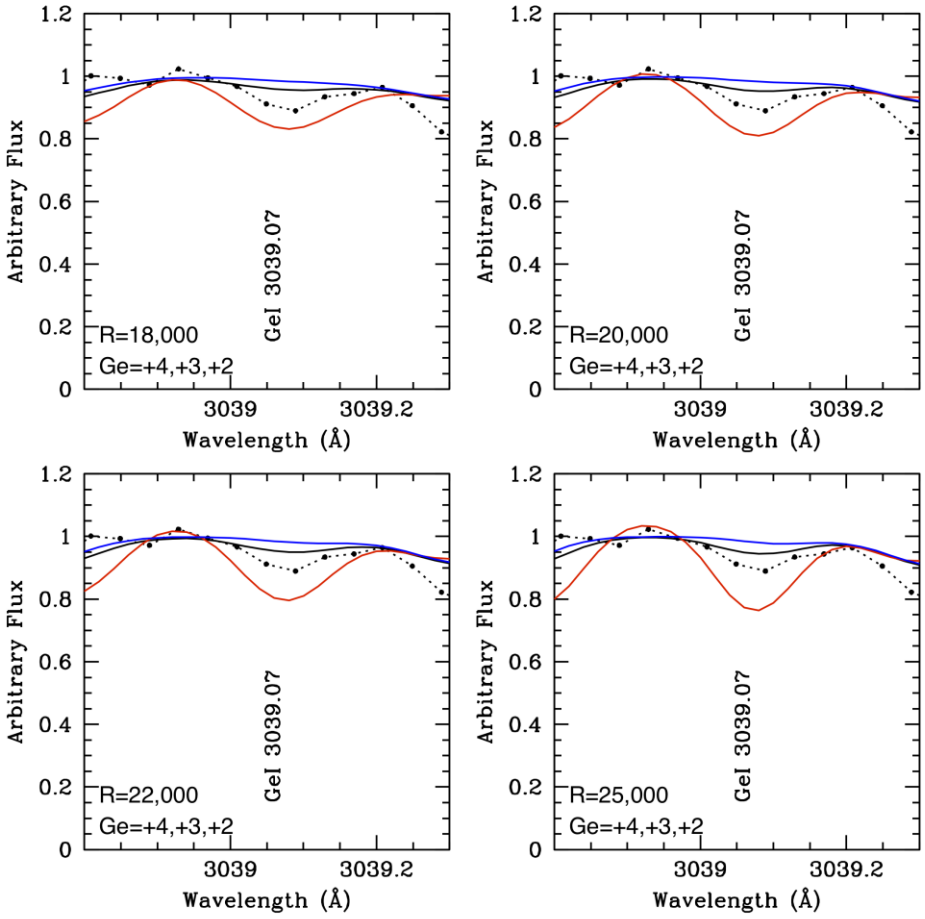

Figure 3: The example of GeI λ303.907nm; the line observed with HST/STIS (black dotted line, Siqueira Mello Jr et al. 2012, submitted) compared with synthetic spectra computed with abundances A(Ge) = +2, +3, +4, at spectral resolutions of R=18,000, 20,000, 22,000, 25,000.

6.3 Carbon, nitrogen and oxygen abundances from molecular lines

The elements carbon, nitrogen, and oxygen are the most abundant after hydrogen; and carbon and oxygen are the first abundant elements to be formed by nucleosynthesis after H and He. Consequently, they are key elements in studies of the chemical evolution of the Galaxy and galaxies in general, as well as in studies of stellar evolution.

The main nitrogen indicator used in the literature are CN bands, among which the strongest ones are in the near-UV, in particular CN(0,0) at 388.3 nm. For the use of CN, one has to previously derive C, available in the optical from the CH G-bandhead at 431 nm or a weak C_2(0,0) bandhead at 563.5 nm. In the near-UV, however, there is the unique available strong NH bandhead at 336 nm (see Figure 4). The NH band measurement in important samples would allow a direct measurement of nitrogen (e.g. Pasquini et al. 2008).

Oxygen also has important indicators in the near-UV, several (around 40) strong OH lines occurring in the range 300 – 330 nm. In metal-poor turn-off dwarf stars, the UV OH lines are the only ones that are measurable.

Therefore, the situation regarding CNO is: with C measured in the optical, generally from the CH G-bandhead at 431 nm, it is then used to derive N from CN bandheads, the strongest ones found in the near-UV. Nitrogen is even better derived, directly from UV NH bandheads, the strongest of which is at 336 nm. Note that there are discrepancies between the CN and NH indicators that need to be better understood.

Oxygen abundances can be derived from 4 sets of lines: (i) the forbidden [OI] λ630.031, λ636.379 nm lines measurable in giants of [Fe/H] >−3.0; (ii) the permitted OI λ777.196, λ777.418 and λ777.540 nm lines measurable in dwarfs and subgiants, or in supergiants the weaker triplet at λ615.603, λ615.680 and λ615.817 nm; (iii) the ultraviolet (UV) OH lines ($A^2\Sigma - X^2\Pi$ electronic transition); (iv) the infrared (IR) OH lines ($X^2\Pi$ vibration-rotation transition). The importance of the near-UV OH lines applies mainly to metal-poor turn-off dwarf stars, in which these OH lines are the only ones of the lines listed above, that are strong enough to be measurable in these stars (see also Figure 5).

More studies on NH and OH lines are needed in terms of line lists and molecular constants, and this basic aspect could be one of the first aims of the proposed UV spectrograph.

Typical S/N ratios for the study of the NH bandhead and OH lines are at least S/N ~ 50. Spectral resolution required is comfortable with R>18,000. Conclusions on the instrument requirements are given in Section 6.4.6 together with the results form the Be line.

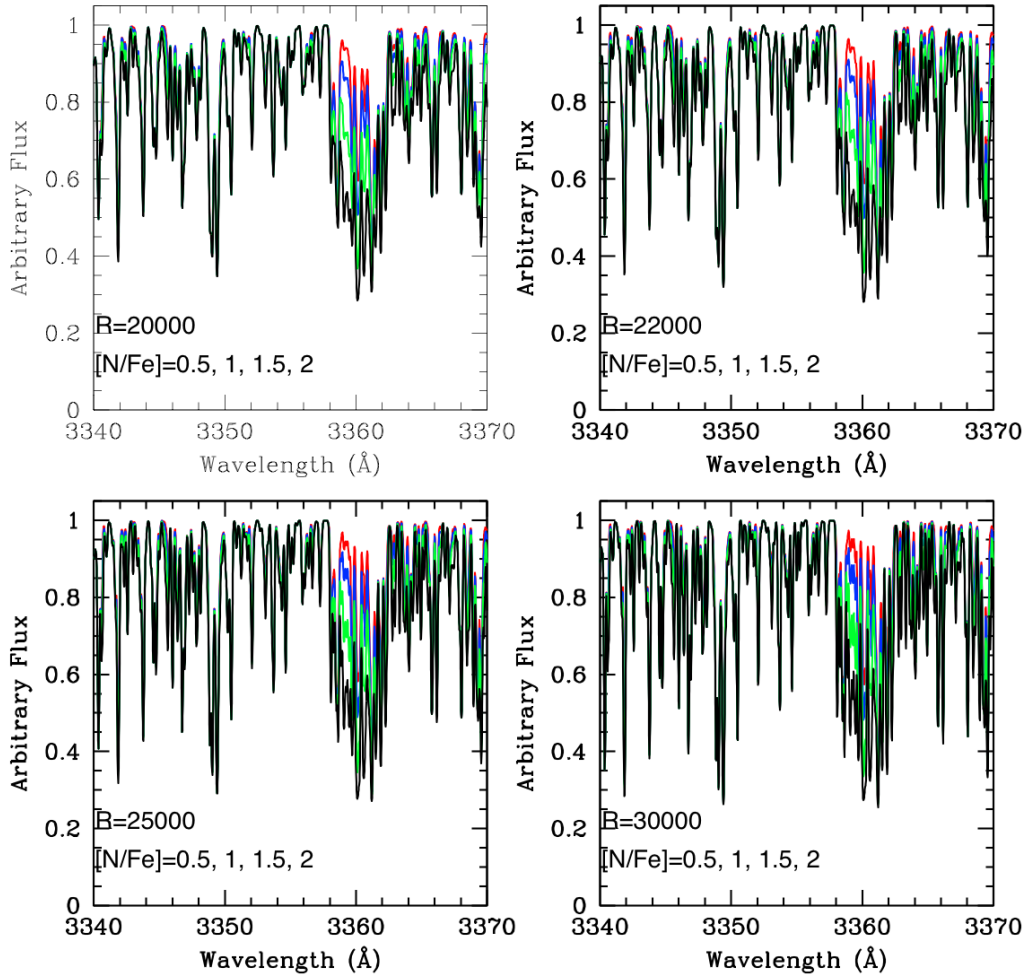

Figure 4: Simulations of the NH bandhead at 336 nm for different spectral resolutions and a metal-poor star of metallicity [Fe/H] = -3.0. The colored lines reflect different [N/Fe] ratios as given in the figure insets.

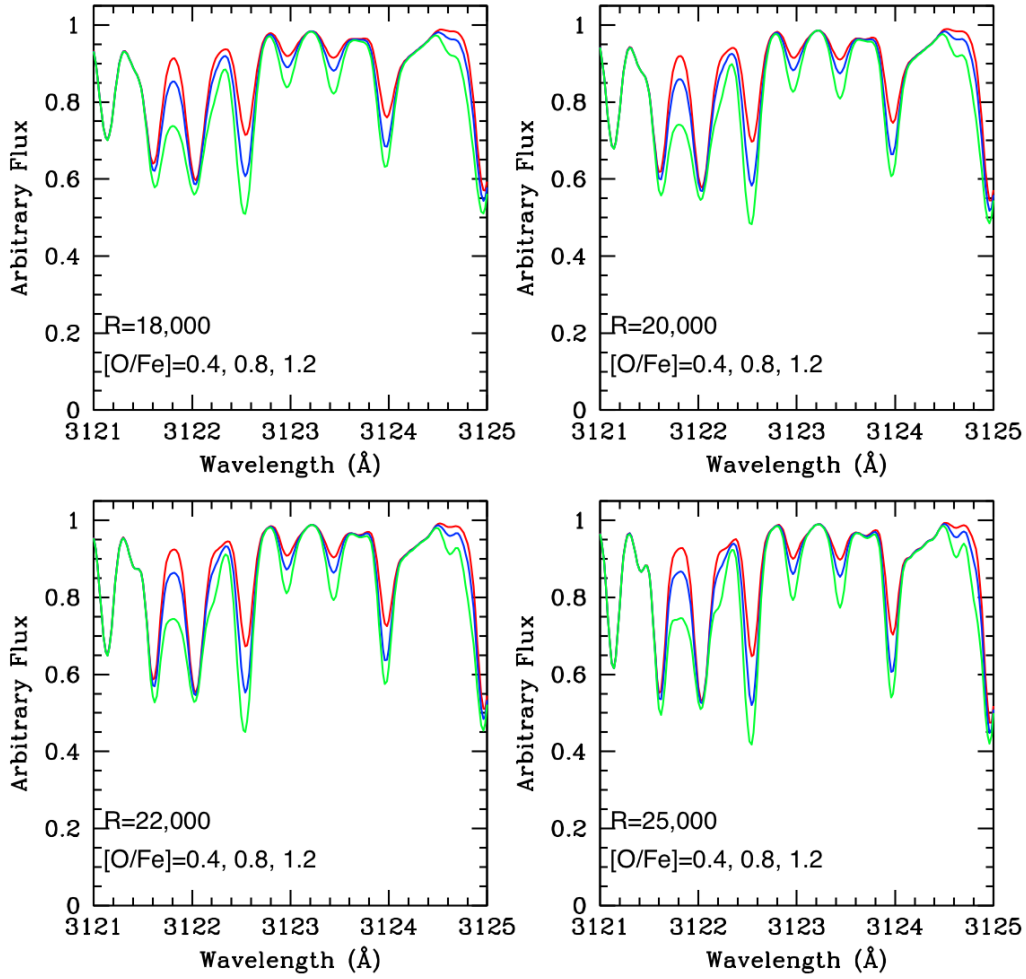

Figure 5: Example of OH lines at 312.3nm for a metal-poor star of [Fe/H] = -3.0. We provide simulations showing a range in spectral resolution and [O/Fe]. There are around 40 OH lines in the 300-330nm region.

6.4 Beryllium

UV is our only spectral window for the determination of Beryllium (hereafter Be) abundance with the Be II resonance lines at 313.042 and 313.107 nm. In order to measure these lines a minimum spectral resolution of about R ~20,000 is needed (see Figure 6). In the following we outline four noteworthy science applications for Be.

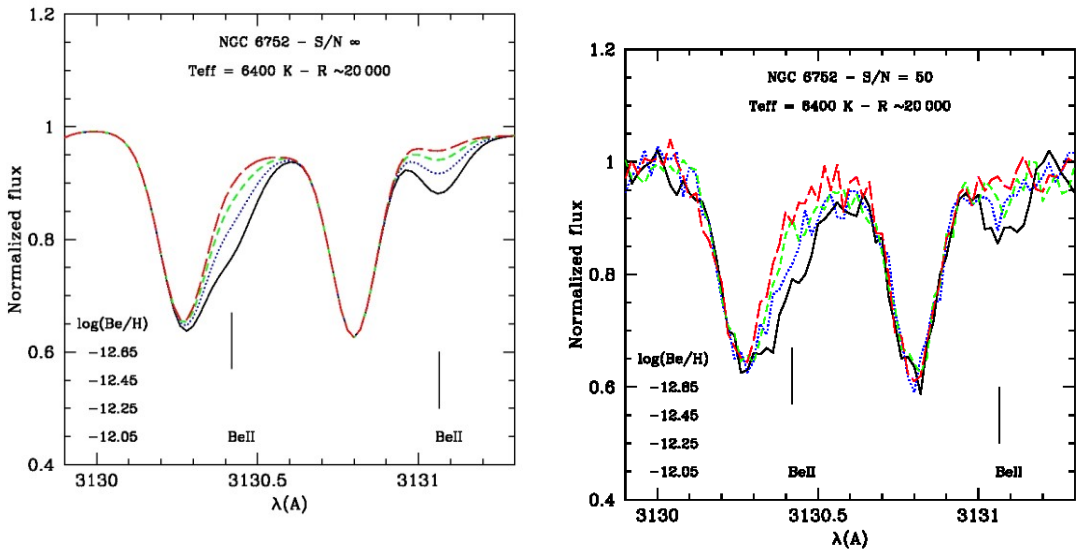

Figure 6: Simulated spectra for a turn-off star in the globular cluster NGC 6752 at R ∼20,000 and varying Be abundance (increasing from dashed red, dashed green, dotted blue to solid black lines). The left plot shows the noise-free simulation while on the right a S/N =50 is shown. Simulations carried out by R. Smiljanic.

6.4.1 Using solar twins to constrain Li and Be depletion

In order to test solar models of Li depletion, theoreticians require stars that differ only slightly from the Sun in mass, age, rotation and metallicity, thus their theories can be safely applied under slightly different conditions. Solar twins are crucial in this regard, because being so similar to the Sun the general principles used for the solar model are still valid for them. Note that this assumption breaks down quickly for solar analogs with masses 10% higher than solar, because they will develop a convective core, thus changing radically the stellar interior description. For many years the Sun has been the cornerstone for stellar astrophysics, it is now the time to also reverse this feedback, where other stars contribute to the understanding of physical processes that are relevant to the solar interior model.

Beryllium is important to constrain the mechanisms (e.g. mass, age, convection treatment, extra-mixing mechanisms, mass loss, metallicity) that destroy Li in the Sun and solar twins, because it allows independent tests of the models required for Li depletion. The expected depletion of Be is much smaller than Li because Be is destroyed at higher temperatures. Empirical evidence shows that the depletion of Be is about one third of the depletion of Li (Boesgaard & Krugler 2008, hereafter BK08), thus high S/N data are needed.

The most recent study of beryllium in ”one-solar-mass” stars based on Keck HIRES data, shows that the Sun may be Be-rich (BK08), although this result should be taken with caution, as their ”one-solar-mass” stars may not be similar to the Sun. Indeed, as shown in their Fig. 1, all their solar analogs studied for beryllium have $M_V < 4.5$, while the Sun has $M_V = 4.81$, i.e., the Sun is likely less massive than their one-solar-mass comparison sample. Nevertheless, the result

obtained by BK08 is quite puzzling: how can solar-analogs have less Be and more Li than the Sun? If their Be abundances are lower, then Li should be even more depleted, since Li is easier to destroy than Be.

However, no beryllium data is available yet for solar twins to confirm or disprove the apparent Be peculiarity described above. Solar twins have not been targeted in the past because they are extremely hard to identify. Besides, they are much fainter than solar analogs making them more challenging targets for UV spectroscopy. A recent spectroscopic survey of solar twins (Meléndez et al. 2009) has identified the best sample of solar twins available; they can provide new insights into the apparent anomalies in the solar Li and Be abundances and provide stringent constraints in the modeling of Li and Be depletion.

6.4.2 Mixing and stellar physics

Lithium abundances have been extensively used in the literature as a way to study mixing between the surface material and the interior of stars. Standard stellar evolution, which only allows for mixing in convective layers, fails to explain nearly all Li abundance patterns observed so far at the surface of low-mass stars. Some of the effects uncovered by the observations are: 1) The vast majority of F- and early G-type stars (including the Sun) deplete Li during their stay on the main-sequence (Sestito & Randich 2005), 2) the Li-dip, a strong decrease in Li abundances of main sequence stars in an interval of ~300 K around ~6700 K (Boesgaard & Tripicco 1986), 3) the presence of a spread of Li among solar-type stars in old clusters like M67 and in field stars (Pasquini et al. 1997), 4) Li dilution starting in subgiants before the first dredge-up (Lebre et al. 1999), 5) the star-to-star scatter in Li and the Li-rotation connection in open clusters and associations both younger and slightly older than the Pleiades (100 million years; Soderblom et al. 1993).

These observations reveal the action of physical processes beyond convection. Many different physical mechanisms have been proposed to explain these observations: atomic diffusion, mass loss, magnetic fields, rotation-induced mixing, mixing by internal gravity waves, or combinations of some of these processes. To help constrain the nature and description of the transport mechanisms of chemicals and angular momentum inside low-mass stars it is important to combine Li data with Be abundances (Smiljanic et al. 2010, 2011). This is possible because, as noted in section 6.4.1, Li and Be burn at different temperatures, namely $\sim 2.5\times10^6$ K for Li and $\sim 3.5\times10^6$ K for Be, these in turn correspond to different depths in the stellar interior.

Beryllium has been investigated in far fewer stars than Li, essentially because Be abundances can only be determined from the Be II resonance lines at λ313.1065 and λ313.0420 nm, a spectral region near the atmospheric cutoff and thus difficult to access with non-optimized spectrographs.

6.4.3 Be as a cosmochronometer

The single stable isotope of beryllium, ^{9}Be, behaves as a primary element in the early Galaxy and is a pure product of cosmic-ray spallation of heavy (mostly CNO) nuclei in the interstellar medium (Reeves et al. 1970). Assuming cosmic-rays to be globally transported across the Galaxy, the Be production can be considered as a widespread process and its abundance should be rather homogeneous at a given time in the early Galaxy. It should have a smaller scatter than the products of stellar nucleosynthesis. Thus, Be should show a good correlation with time and could be employed as a cosmochronometer for the early stages of the Galaxy (Suzuki & Yoshii 2001, Pasquini et al. 2005).

Together with abundances of oxygen (or alpha elements), Be can be used to investigate the evolution of the star formation rate in the old Galactic components (halo and thick disk). The idea is to use a diagram of [O/Fe] vs. log(Be/H) where the abscissa can be considered as increasing

time and the ordinate as the star formation rate. A division of stars into two components can be interpreted as a difference in the time scales of star formation. It is important here to observe main sequence stars with undepleted Li, that also did not deplete their initial Be abundance.

For example, the halo stars analyzed in Smiljanic et al. (2009) were shown to split into two components in a diagram of [O/Fe] vs. log(Be/H), revealing two components with distinct star formation histories. Although the interpretation is still open, the result shows that the halo is not a single uniform population with a single age-metallicity relation. The difference may be related to the accretion of external systems or to variations of star formation in different and initially independent regions of the early halo. A similar division was found by Nissen & Schuster (1997, 2010) but using Fe as a tracer of time. The division seems clearer when Be is used as a time scale, Be can thus contribute to improving our knowledge of the processes of the Galaxy formation (see e.g. Tan & Zhao 2011). Larger samples of kinematically selected metal-poor stars are needed to better understand the detailed behavior of Be in the Galaxy, its use as a cosmochronometer, and as a discriminator of stellar populations.

Detections of Be in extremely metal-poor stars ([Fe/H] ~−3.00) suggest a possible flattening of the relation log(Be/H) vs. [Fe/H], that could be seen as a plateau (Primas et al. 2000a; 2000b). However, there are only a few stars in this regime with determined Be abundances and other authors have questioned the existence of the flattening (see e.g. Boesgaard et al. 2011). All other known stars with this or lower metallicity are too faint to be observed with current instrumentation. Observation of larger samples with data of better quality is needed. Only then it will be possible to extend the analyses to lower metallicity and better constrain the possible presence of the plateau and its characteristics. In this case, however, the lines will have very low equivalent widths, therefore the relatively low resolution could be an issue here. There are several scenarios that can produce a Be plateau such as: 1) a significant production of Be in an inhomogeneous primordial nucleosynthesis; 2) pre-Galactic production by cosmic-rays in the intergalactic medium; 3) accretion of metal-enriched interstellar gas onto metal-poor halo stars, while crossing the Galactic plane.

6.4.4 Be and the formation of Globular Clusters

All the globular clusters analyzed with sufficient depth so far show signs of chemical inhomogeneities in the light elements (Li, C, N, O, Na, Mg, and Al; see e.g. Gratton et al. 2004). These manifest as typical signatures of material processed by proton-capture reactions. It is now accepted that this material was produced by a previous generation of stars that polluted those that are observed now, although the nature of these polluters is still debated (massive AGBs or fast-rotating massive stars; see e.g. Decressin et al. 2007; Ventura & D'Antona 2009).

In this context Li and Be are of particular interest as they are fragile, destroyed in (p,α) reactions in temperatures above ~2.5×10^6 K and ~ 3.5×10^6 K, respectively. Li, however, can be produced in AGB stars via the Cameron-Fowler mechanism while Be is never produced, only destroyed. As the other proton-reactions (CNO and NeNa cycles) require much higher temperatures, the processed material is completely devoid of Be, regardless of the polluter.

In NGC 6397, stretching the UVES capabilities, Pasquini et al. (2004) observed two turn-off stars with much different O and possibly the same Be. In the simple dilution-pollution scenarios currently proposed to explain the chemical properties of globular clusters, Be should always be diluted in O-poor stars, since it is only present in primordial material, not in processed material. If this result could be confirmed, then the current scenario of GC second generation of star formation would have to be abandoned. The proposed UV spectrograph should enable Be determinations in several clusters with different populations, and characteristics, e.g. NGC 6397, NGC 6752, M4, Omega Cen, NGC 2808 (see also Figure 6).

Target considerations

Relevant stars for the globular cluster case have V ~ 17 for the turn-off in NGC6752; in Ω Centauri the two turn-off stars are fainter with B ~ 18.2 and 18.8. For the metal poor star case the typical magnitudes are V = 13 to 15 for the nearer well-known clusters, but at V ~ 15 – 17 in many more further away and fainter clusters.

6.4.5 Spectral resolution and S/N requirements

The discussion on the requirement for minimum spectral resolution and minimum S/N is conducted with the following two science cases:

1) Beryllium abundances in turn-off stars of globular clusters;
2) Beryllium abundances in metal-poor stars with [Fe/H]<-3.0.

Spectra were computed with three different spectral resolutions, R=15,000, 20,000 and 25,000. Four different S/N levels were simulated: S/N=20, 50, 100, 150. These values of S/N are valid for the case of R=25,000. For the other spectral resolutions the S/N was scaled to emulate the gain in S/N given by the decrease in spectral resolution. Therefore the values used were S/N=22, 56, 112, 168 for R=20,000 and S/N=26, 65, 129, 194 for R=15,000.

Case 1 – Beryllium in globular clusters: all globular clusters investigated so far show signs of abundance spread in light elements (Li, C, N, O, Na, Mg, Al). This should be a mix between pristine material and processed material. This gives rise to correlations and anticorrelations seen in stars in globular clusters. Beryllium should behave in the same way. In particular, Be is not produced by stars but only destroyed. Thus the polluting material should be devoid of Be. A star formed with pristine material instead should have the original Be abundance. Stars with different amounts of polluted material should have diluted Be to different levels, the more polluting material, the less Be the star should have. Therefore, in this science case, the aim is to detect differences in Be abundance among different turn-off stars of the same cluster.

In the simulations below, shown for a resolution of R=20,000, each were computed with two different Be abundances. The higher abundance in NGC 6752 is log (Be/H)=-12.05 (Pasquini et al. 2007, A&A, 464, 601), and a lower abundance by 0.60 dex are adopted. For Ω Centauri, the Be abundances were scaled according to the metallicity, therefore log (Be/H)=-13.2. A solar Be abundance of A(Be)=1.10 was adopted, and alpha-elements are assumed to be enhanced by [alpha/Fe]=+0.4.

Simulations apply to two different stars:

- Turn-off star in NGC 6752: T_{eff} = 6400 K, log g = 4.30; [Fe/H]=-1.50, v_t=1.20 km/s (see Figure 7)
- Turn-off star in Ω Centauri: T_{eff} = 6700 K, log g = 4.20; [Fe/H]=-2.00, v_t=1.20 km/s (see Figure 8)

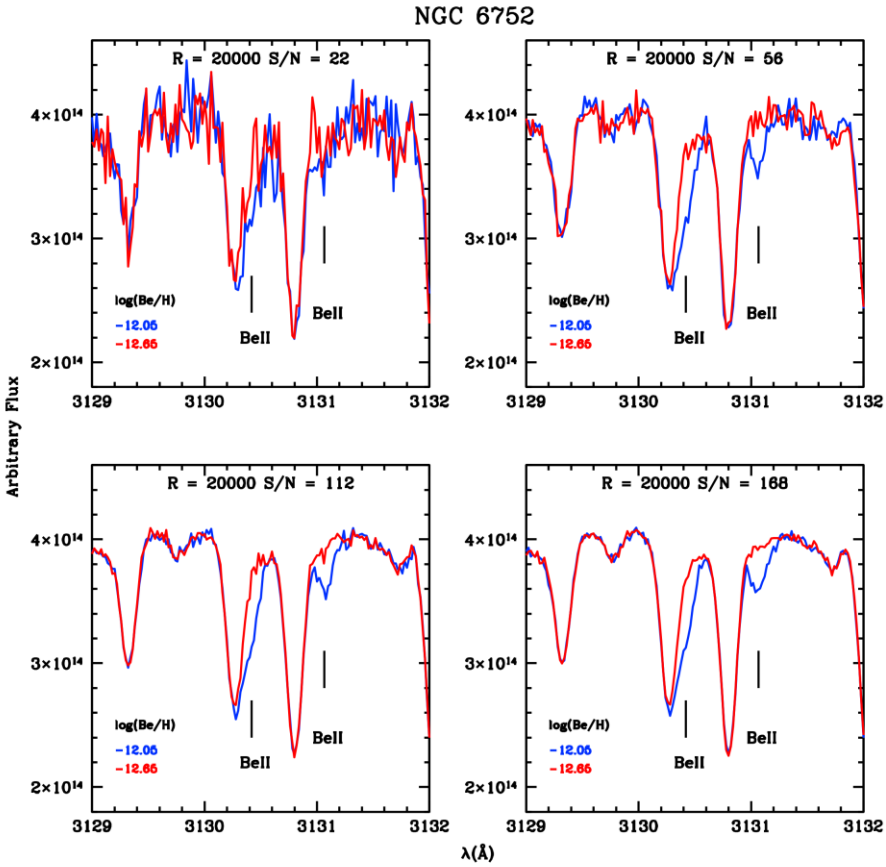

Figure 7: Comparison between turn-off stars of NGC 6752 with R=20,000 as function of S/N. A difference in abundance of ΔBe = 0.60 dex can be detected for S/N >50.

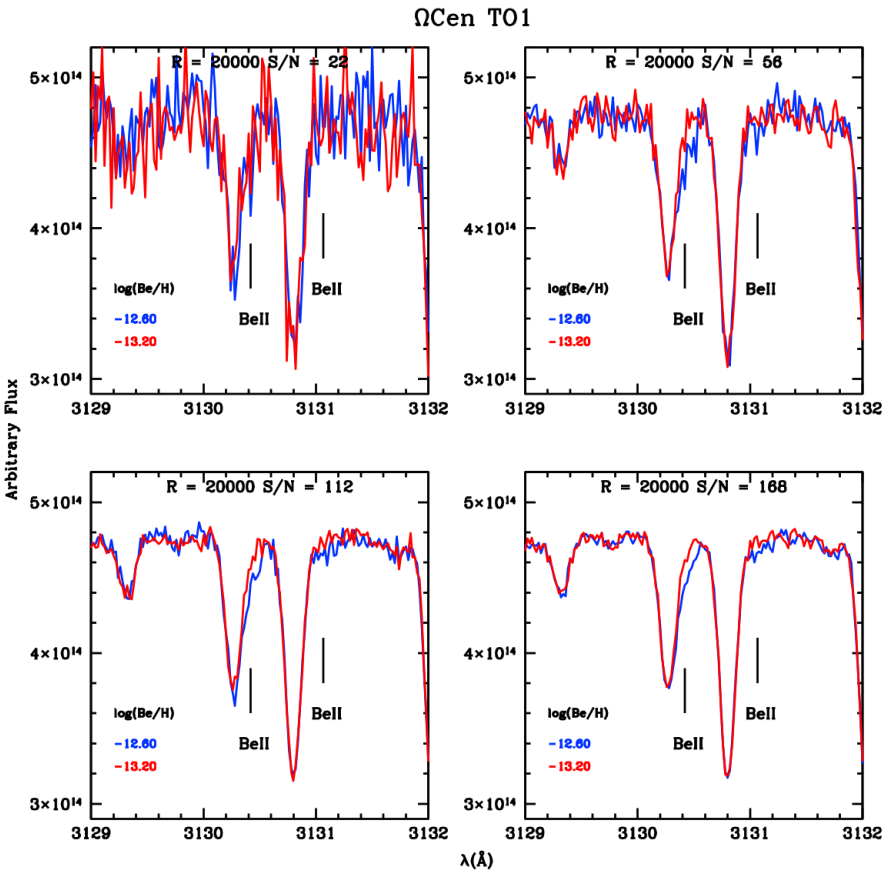

Figure 8: Comparison between stars at the metal-poor turn-off of Ω Centauri with R=20,000. A difference in abundance can be detected for S/N >100.

Case 2 – Beryllium applied to extremely metal-poor stars:

Detections of Be in extremely metal-poor stars ([Fe/H]<-3.0) suggest a possible flattening of the relation log (Be/H) vs. [Fe/H]. This could in principle be interpreted as a plateau at low metallicities, similar to the Li plateau. However, there are Be measurements for only a few stars at these low metallicities. Other candidates are too faint to be observed with current instruments. Therefore the higher throughput of the proposed UV spectrograph would perfectly fit to such a scientific aim.

Spectra of two different stars were simulated, each one with two different Be abundances. The higher abundance for the two stars simulates a plateau, with log (Be/H)=-13.10, as found for G64-12 ([Fe/H]=-3.5), and a second, smaller abundance by 0.60 dex is assumed. The stellar parameters are applied to:

1. T_{eff}=6300 K, log g = 4.30, [Fe/H]=-3.0, v_t = 1.20 km/s (see Figure 9).
2. T_{eff}=6300 K, log g = 4.30, [Fe/H]=-3.5, v_t = 1.20 km/s (see Figure 10).

For metal poor stars the Be lines can be detected if there is a Be abundance plateau (blue lines in Figure 9 and Figure 10). In the absence of a plateau, i.e. if the linear relation between Be and Fe holds at low metallicities, then only an upper limit can be set. For both cases S/N ratios of at least 100 are required at 313 nm.

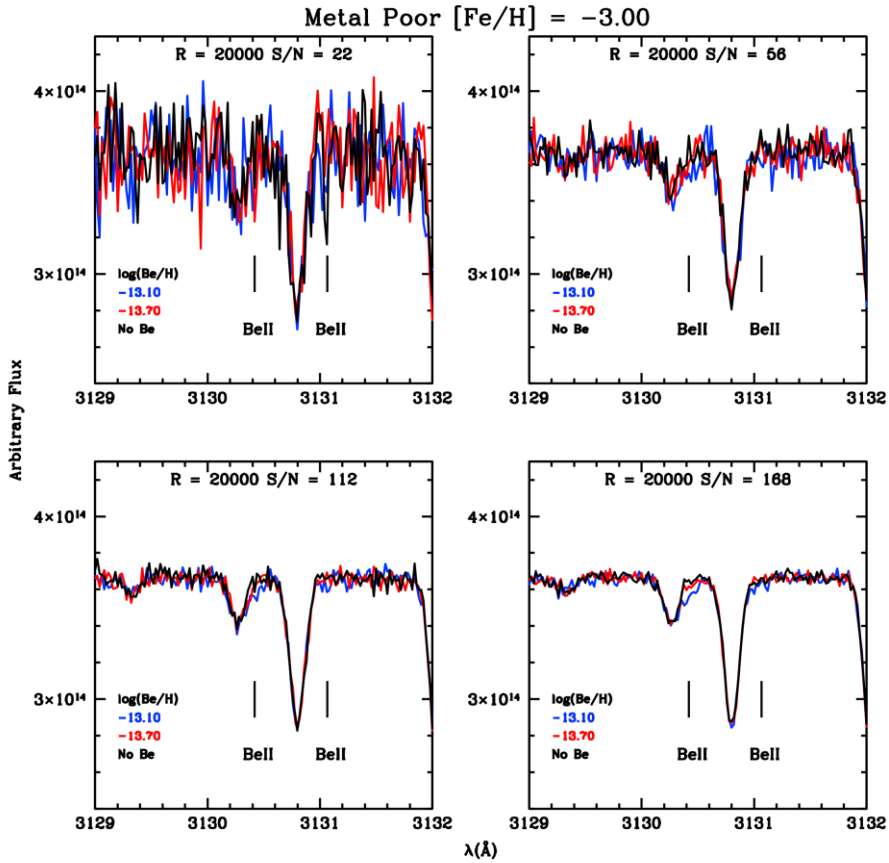

Figure 9: Comparison of three spectra of a metal-poor star with [Fe/H]=-3.0 at R=20,000. The black spectrum was computed with no Be, the blue with log (Be/H)=-13.10 and the red one with a lower abundance by 0.60 dex.

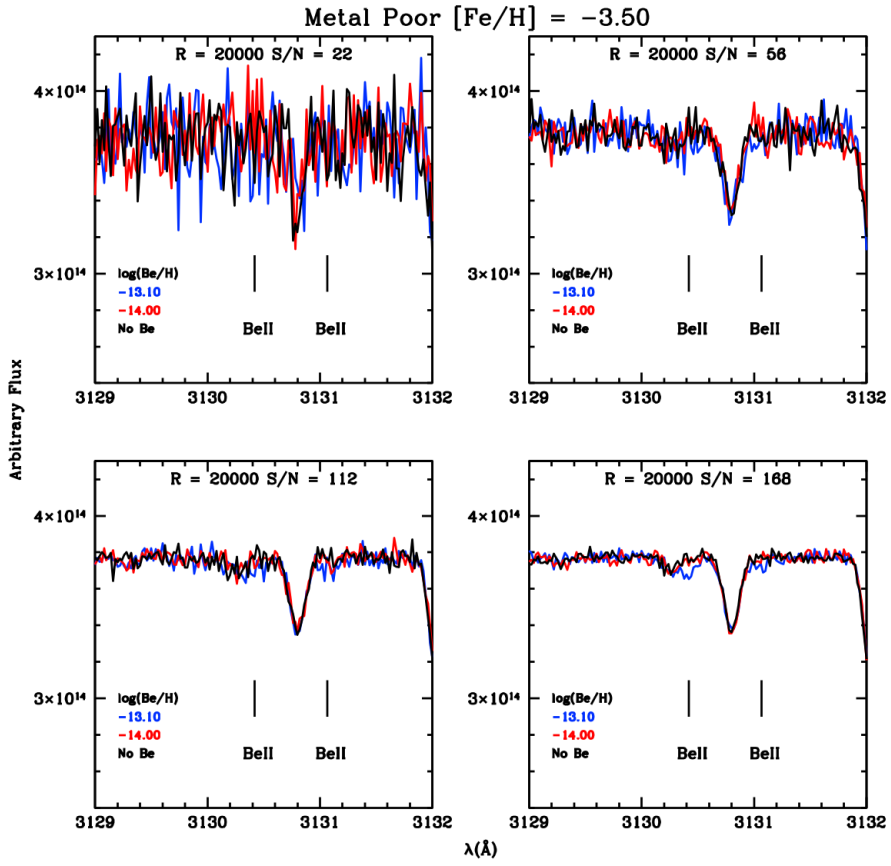

Figure 10: Comparison of three spectra of a metal-poor star with [Fe/H]=-3.5 at R=20,000. The black spectrum was calculated without Be, the blue with log (Be/H)=-13.10 (simulating an abundance plateau), and the red one with an abundance decreased by 0.90 dex.

6.4.6 Instrument requirements

The analysis by Beatriz Barbuy and Rodolfo Smiljanic shows that a spectral resolution of R~20,000 is sufficient for the Be case and the large majority of metal lines or bandheads considered in Sections 6.2 and 6.3. Only UII λ3859.57 would require R>30000 and will need to be covered with other instrumentation (e.g. UVES, ESPRESSO). Particularly the Be case shows that high signal-to-noise ratios (>100) and therefore spectrograph performance and specifically throughput is of paramount importance.

Therefore the spectrograph and operational concept must allow for the possibility of long exposures (i.e. 45min exposure time) and the possibility to co-add several (up to ~10) exposures. In order to avoid degradation of spectral resolution and optimisation of the SNR the stability of the spectrograph should be better than 1/5 pixel in wavelength direction and better than ½ pixel in cross-dispersion direction (including atmospheric dispersion effects).

Additionally, the noise contribution (read-out noise [RON], dark current) of the detector system is a critical parameter for faint sources and should not exceed the one from the sky for long exposures. For example, using the preliminary ETC with the following setup (point source, K0V template, V=17.5, airmass=1.3, exposure time 1800s, reference wavelength 315nm) the noise contribution from the source and sky is sqrt(60) e- and sqrt(52) e-, respectively. Therefore, the detector contribution should be of order sqrt(60) e- or less, translating in detector requirements of RON < 3 e-/pixel/DIT and a dark current rate of < 0.001 e-/pix/s.

6.5 Analysis of Planetary Nebulae in the UV

Accurate chemical abundances of several elements that can be difficult to study in stars can be obtained from emission lines of planetary nebulae (PN), especially concerning the elements He, C, N, O, Si, S, and Cl. Apart from optical and infrared lines, several of these lines are in the ultraviolet. In the range 300−400 nm several important emission lines can be measured in PN, mostly collisionally excited lines such as [O II] λ372.6, λ372.9, O III λ302.3, λ304.3, λ313.3, [Ne III] λ386.9, [Ne III] λ334.3, λ387.0, λ396.7, λ396.8, [N II] λ306.3, [NI] λ346.7, [S III] λ372.2, λ379.8, [C III] λ358.7, λ367.8, [Cl III] λ334.3, λ335.4, [Cl IV] λ311.9, λ320.4, [Ar III] λ300.6, λ311.0 nm. These lines can be used to determine the ion abundances of the corresponding elements and the electron temperature in the case of the [O II] line, especially when other optical (or infrared) lines are available. Some Bowen fluorescence lines can be produced in specific environments, including O III λ313.3, λ334.1 and λ344.4nm. Some recombination lines of abundant elements are also often observed, such as O III λ326.5nm, He I and H8 λ388.9nm Hε λ 397.0 nm. At effective temperatures in excess of 30000 K, the PN central stars emit most of their radiation in the ultraviolet, peaking around 120 nm, with measured radiation up to about 320 nm.

There are over 2000 planetary nebulae known in our Galaxy, with many more observed in the galaxies of the Local Group, especially in M31 and the Magellanic Clouds. Presently, there are relatively accurate abundances measured for a few hundred Galactic nebulae, which will constitute the main initial targets for the UV studies (see for example Milanova and Kholtygin 2009, Stanghellini et al. 2005). Also, recent studies of the central stars based on UV measurements have given a powerful insight into the strong stellar winds observed in these stars, particularly those that are H deficient, both for the Galaxy and the Magellanic Clouds (Herald and Bianchi 2004ab).

The above science does not set stringent requirements on the spectral resolution, but the measurement of emission line abundances requires a reasonably accurate flux calibration.

6.6 Novae, close binaries and compact stars

In the following we outline several science opportunities which arise from the proposed UV spectrograph in the area of novae, close binaries, and compact stars.

1. **Precision accretion column tomography using weak high ionization lines:** Magnetically funneled mass transfer in close binaries can be studied using tomographic reconstructions of the gas flow by measuring emission line profiles along the orbit. High ionization metal lines like N IV λ3479, 3483, 3485 are expected to be weak. However, their profiles may reveal the column structure close to the accreting white dwarf, probing the presence of magnetic quadrupoles. Dozens of potential targets are available in the southern hemisphere.

2. **Transient Heavy Element Absorption Systems in Novae:** Short-lived absorption line systems were recently discovered in recent high-resolution observations of classical novae outbursts (Williams et al. 2008) while probing the circumbinary medium around classical novae using Transient Heavy Element Absorption (THEA). Single ionized lines of Sc, Ti, V, Cr, Fe, Sr, Y, Zr, and Ba are possibly formed in a circumbinary gas. Chemical abundances and mass loss rates in this gas are essential to the understanding of binary evolution and production of SNIa in those systems. Many of these lines can be conveniently observed in the UV range, beyond the Balmer jump in emission. 2 to 6 classical and recurrent novae per year are expected to present measurable THEA systems.

3. **Velocity structure of neon lines in recurrent novae:** The presence of strong neon lines in recurrent novae is an indication of a CV (cataclysmic variable) SNIa progenitor. The evolution of the UV NeIII and NeV line profiles and flux can be used as a constraint to 3D photo-ionization models of the nova shell. Such models provide the best estimate of the mass loss in outbursts defining the evolution of the white dwarf close to the Chandrasekhar limit. The kinematics and mixing of neon in the ejecta is key to understanding how nova outbursts change along time as the white dwarf gravity increases. Recurrent novae are rare systems - about 20 objects are currently known. U Sco has strong neon lines and regular recurrences every 10 years.

4. **Spectral signatures of planets or small bodies accretion in white dwarfs:** High resolution and high S/N observations of the blue and UV continuum of white dwarfs may reveal the presence of metals with a short diffusive time-scale indicating recent accretion of material of planetary/asteroid origin as seems to be the case in GD 362 (Jura et al. 2009). The observation of metal lines in the UV has advantages regarding the absence of Zeeman-split components and brighter continuum. Precise atmospheric density diagnostics for those WDs of the DA type can be also made in the UV by using the Inglis-Teller method. The search for suitable planet accreting WDs candidates can be pursued by taking into account their infrared and X-ray properties.

Medium to high resolution studies of the emission lines observed during the early evolution of classical novae are important to understand the companion irradiation effects (Diaz et al. 2010), the white dwarf accretion process after outburst and the ejection velocity distribution. In all cases, the line profiles may present structures that are resolved with resolution R> 15,000 - 20,000. In general, the science case of Nova outburst kinematics is not, by itself, a driver for high resolution. On the other hand, the profiles of forbidden lines in the UV are key to study stratified ejection in high mass (ONeMg) white dwarfs, which are considered a candidate path to LMXB by core induced collapse. Important [NeIII] diagnostic lines are at 334.3, 386.9 and 396.8 nm. Highly

ionized shells may present [NeV] lines at 334.6 and 342.6nm. Therefore, a wavelength coverage from 330 to 400 nm is desirable for nova outburst studies. Of course, the velocity resolved diagnostic of photoionized nebulae in other astrophysical scenarios would also benefit from such an extended coverage.

6.7 Bowen effect in Symbiotic stars, PN, AGN, and X-ray binaries

For a long time (Bowen 1934, 1935), it has been recognized that some O III permitted emission lines seen in planetary nebulae (PN) are produced essentially by the so-called Bowen fluorescence mechanism. This mechanism consists in the excitation of the $2p^2\,{}^3P^o$ level of O III by the *Lyα* line of He II at 30.378 nm (in a remarkable coincidence the transitions $2p^2\,{}^3P_2$ - $2p3d\,{}^3P^o_2$ and $2p^2\,{}^3P_2$ - $2p3d\,{}^3P^o_1$ of O III rest respectively at 30.380 and 30.369 nm). Subsequent cascades of the $2p3d\,{}^3P^o$ level to the $2p3p\,{}^3P$, $2p3p\,{}^3S$ and $2p3p\,{}^3D$ levels yield the "main Bowen" lines, and further decays from those $2p3p\,{}^3L$ levels to the $2p3s\,{}^3P^o$ level create the "subordinate" lines. The subordinate lines can also be excited by other processes, such as charge transfer of O IV in collision with neutral hydrogen and/or radiative and dielectronic recombination (Liu, Danziger & Murdin 1993).

As a consequence of Bowen fluorescence several emission lines can be detected between 310 nm and 410 nm and between 370 and 570 nm. Therefore, the study of Bowen lines in symbiotic stars and other gaseous nebulae can be useful to probe the physical conditions under which these lines are formed and also measurements of the Bowen efficiency can be compared with photo-ionization models.

Instrument Requirements

This science case does not pose any significant constraints over and above the leading stellar cases and as such parameters are covered elsewhere.

6.8 Surface gravity determination with hydrogen and helium lines

The wavelength range of the proposed UV spectrograph covers the H I Balmer edge at 364.6 nm. The strength of the so-called Balmer jump (flux ratio directly before and after the threshold) was used at the beginning of spectral analyses to determine stellar temperatures.

Modern spectral analyses are based on LTE (for stars with spectral type B or later) or non-LTE model-atmosphere techniques that provide reliable spectral energy distributions. These are then compared with observations. Subsequent fine-tuning of basic parameters like effective temperature, surface gravity and elemental composition is performed to achieve best agreement.

While the determination of the effective temperature is based on the evaluation of ionization equilibria and thus, very precise, the determination of the surface gravity is done by detailed comparison of line profiles. Unfortunately, for most metal lines, no reliable Stark-broadening tables are available and therefore, mainly hydrogen and helium lines in the optical wavelength range are used. Since the lower members of the spectral series form more outside in the atmosphere, they are strongly dependent on the precise determination of the metal abundances (neglecting metal opacities leads e.g. to the so-called Balmer-line problem; Napiwotzki & Rauch 1994; Werner 1996). The higher Balmer series members (going to the HI Balmer edge) form deeper inside the atmosphere and are more reliable. Since the quality of most available spectra is rather poor close to the HI Balmer edge, the error range of this surface-gravity measurement is relatively large, especially for hot post-AGB stars (see Figure 11, with a typical error ellipse). These targets are important since in their AGB phase, stars of intermediate mass (0.8 - 8 solar

masses) lose up to 90% of their initial mass by stellar winds. The ISM ingests the nuclear processed material that is mixed up to the stellar surface during the thermal pulses on the tip of the AGB. Presently this metal enrichment process dominates in our Galaxy that by supernovae by an order of magnitude. Spectral analysis of post-AGB stars thus provide a crucial test for stellar evolutionary theory and the chemical composition of the stellar outer layers and winds.

The H I Balmer lines approximately coincide with lines of the He II Pickering series that, in case of hydrogen-deficient stars, can be evaluated for the surface-gravity determination as well. The UV spectrographs wavelength range covers the He II λ320.402nm line (Fig. 12, n - n' = 3 - 5) of the He II Fowler series that, together with He II λ468.701nm (3 - 4, from other optical spectra), providing then an additional strategic decrement to evaluate.

Spectra with a spectral resolution of R ≥ 10,000 and a typical S/N of 50 to 100 around the Balmer edge (we would prefer wavelength coverage at least up to 400nm for the red end) provide the opportunity to evaluate the Balmer decrement precisely (see Figure 12 and Figure 13, cf. Rauch et al. 1998, A&A, 338, 651, their Fig. 10). This will reduce the error in surface gravity by at least a factor of two. The errors of the abundances will reduce accordingly. In addition, e.g. Ne VII 364.4nm (Werner, K., & Rauch, T. 1994, A&A, 284, L5) lies in this wavelength range. Neon is a key element for the study of the late He-shell flash phenomenon that drives the evolution of, e.g., Sakurai's object and FG Sge. In the CUBES wavelength range some O IV multiplets are located (338.1 - 375.8 nm) that provide the only possibility to measure the oxygen abundance of these objects.

Targets, typically have magnitudes in the range V = 15 – 19. Suitable are in general, all stars with high log g (≥ 5 in cm/sec^2), e.g. 1316 CSPN selected from Kerber et al. (2003) but all (pre-)white dwarfs are worthy targets as well (see Gianninas et al. 2011).

Instrument requirements

This science case would be ideally covered with a wavelength range between 310 – 420 nm at a spectral resolution of R ≥ 10,000. Suitable S/N ratios are in the range 50 to 100. Any detector gaps should be placed well away from the H I Balmer edge at 364.6 nm (as a goal only one gap at < 360nm).

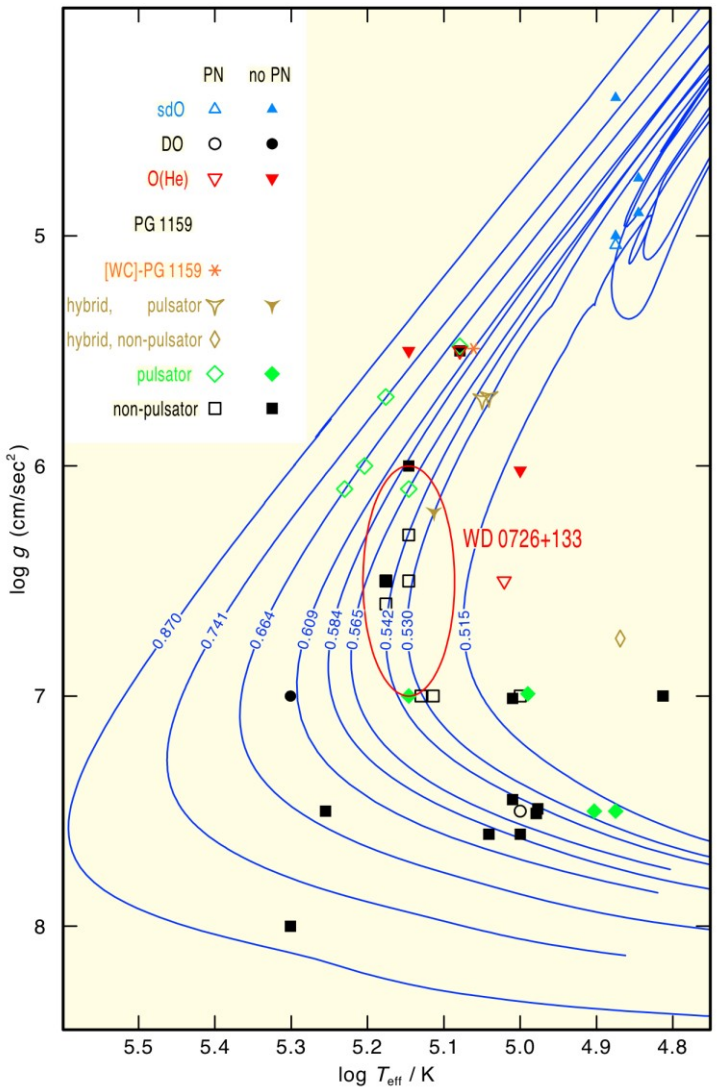

Figure 11: Location of hot post-AGB stars in the log Teff - log g plane compared with evolutionary tracks of hydrogen-deficient post-AGB stars (Miller Bertolami et al. 2006). The ellipse indicates the present, typical error range of spectral analyses based ion non-LTE model-atmosphere techniques.

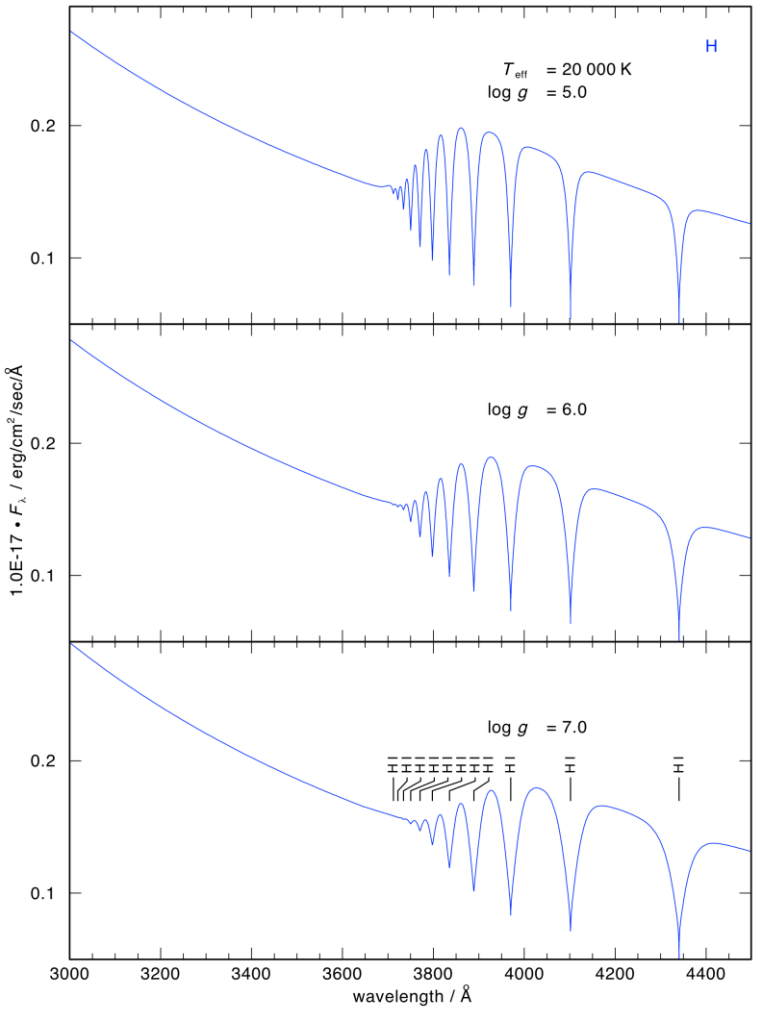

Figure 12: Surface-gravity dependence of the H I Balmer decrement towards the edge. The pure-H models have T_{eff} = 20 000 K and log g = 5, 6, 7.

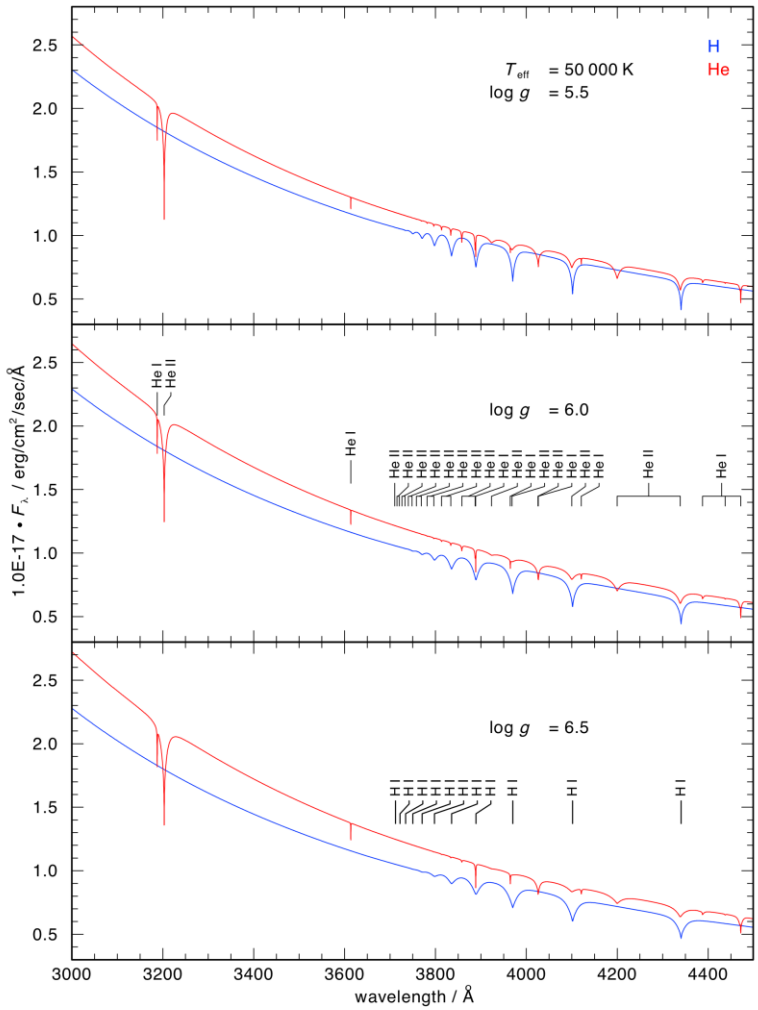

Figure 13: Same as Fig. 11 for models with T_{eff} = 50 000 K and log g = 5.5, 6.0, 6.5 (blue: pure-H models, red: pure-He models).

6.9 Interstellar matter

[Contributions to this case were kindly provided by Rosine Lallement]

A high-efficiency UV spectrograph would be an extremely valuable new tool for the study of the physical processes at work in the galactic ISM, and would also be ideally complementary to current and forthcoming efforts, in particular it would contribute to the three-dimensional mapping of stars, gas and dust that Gaia and associated spectroscopic surveys from ground will make feasible during the next decade. As a matter of fact, the unexplored 310 – 390 nm interval is known to possess gaseous lines of prime interest for both theoretical reasons and mapping purposes. Moreover, this domain has never been investigated in depth for the detection of weak or new absorptions, opening new perspectives.

6.9.1 Major near-UV interstellar lines from the gaseous

The following atomic lines in the range 300 – 400 nm (for completeness we add features up to 430nm noted by an asterisk) are relevant for the present science case: BeII (313nm), NaI (330nm), AlI (394nm), KI (344nm weak, 404nm*), CaI (423nm*), CaII (393-397nm), TiI (363nm), TiII (323,324,338nm), V I (318 to 385nm), Cr I (358-359-360nm), Mn I (403nm*), Fe I (386nm), CoI (352nm), Ni I (323-337nm), Cu I (326nm). Molecular interstellar lines available are CN (387nm), CH (430nm*), CH+ (423nm*), C13H+, OH (310nm band). C3 (405nm*) is also observable, however requires very high signal to noise observations.

Most of the lines below 390 nm have been unexplored. Be II is the dominant state of beryllium in H I regions and its line at 313 nm is the only one available. Be is produced through spallation reactions in the ISM and its abundance is crucial for chemical evolution of galaxies. Inversely, its abundance can be used to test the scheme for the origin of Galactic cosmic rays (see e.g. Prantzos, 2012).

The oscillator strengths of the Na I doublet (around 330nm) are very small and reveal only the strong absorption clouds; for distant ISM observations, they have the strong advantage of not suffering from saturation effects, which is the main problem encountered with the very strong 589nm Na I lines. They will be ideal for ISM mapping (see below), and they also give access to the detailed velocity structure of the line-of-sight, which greatly helps measuring much more precise column densities, of neutral sodium, but also of other elements, by application of the structure. Also, it has been demonstrated that Na I is a tracer of H I and can be used as a proxy available from the ground, contrary to H I only available in absorption in the far UV.

The Ca II doublet (393 and 397 nm) is one of the strongest IS absorption lines. The Ca I line is very strong and together with Ca II provides the ionization fraction of calcium; Ti I and Ti II offer a similar possibility, and, similarly to the near UV Na I lines, Ti is more adapted to strong absorptions than Ca. Neutral sodium traces dense, neutral clouds, while Ca II and Ti II can arise both in cold, relatively dense gas, and also warmer, lower density and ionized gas. On average, the velocity distribution of Ca II is larger than the Na I one; Ca II can trace gas invisible otherwise (many absorption regions have been detected in most of the velocity range between the Milky Way and the Magellanic Clouds thanks to the bright supernova 1987A; Andreani et al. 1987).

Abundances of calcium and titanium, hence their depletion onto dust grains, are important because they are refractory elements and amongst the most depleted ones, contrary to sodium. The Na / Ca ratio (or Na/Ti) is also sensitive to grain disruption. As a matter of fact, all these lines and correlations between them and with others provide lots of information on structures, temperatures, turbulence, ionization, abundances, depletion and cloud physical conditions. All other ions are not always the dominant ones in diffuse ISM, but can be significant.

They offer the possibility to build separate 3D distribution of the molecular content of the IS clouds. CH is sensitive to shocks. CN traces the densest cores. The C12 / C13 ratio available from CH+ is particularly important for the chemical evolution of the ISM and galaxies, and nucleosynthesis models.

Be elemental and C isotopic abundances in the Milky Way disc could reveal important features of some nucleosynthetic processes. It has to be noted that one IS absorption line of CN requires an excitation corresponding to a background temperature around 2.7 K, exactly the temperature of the cosmic microwave background radiation (Kaiser et al. 1990). One could speculate about measuring such molecular lines at different redshifts to reveal the increasing temperature of the Universe when going in the past.

6.9.2 Understanding the physical state of the multi-phase galactic interstellar medium and the processes at work

The interstellar matter plays a key role in the chemical and dynamical evolution of galaxies; it is the raw material out of which stars and planets are formed; it is a source of chemical enrichment of galactic halos and the intergalactic medium. Understanding the physical processes operating in the interstellar medium (ISM) is therefore critically important, but also extremely complicated because the ISM is hugely inhomogeneous and often out of ionization and thermal equilibrium. The nearby ISM provides some kind of prototype for the more general galactic ISM: the Sun is embedded in the 200 pc-wide Local Cavity devoid of gas and dust (see e.g. Welsh et al. 2010, Vergely et al, 2010) whose interior and boundaries show a wide range of temperatures and densities, with most of those structures having been shaped by supernovae and winds from hot stars in local stellar associations. The origin of the cavity is still unclear. At the kiloparsec scale, the local ISM is dominated by the Gould belt, an expanding ring of clouds and stars, whose origin is still debated, too. More generally, although past and present spectroscopic data have begun to answer, several important questions need new UV data for more complete answers.

Is the ISM thermally and dynamically stable?

The total pressure in the mid plane of the Galaxy due to the weight of the overlying material is ten times the thermal pressure, and must be balanced by the sum of the magnetic, cosmic ray, ram and thermal pressures. Recent more realistic 3D MHD models (de Avillez and Breitschwerdt, 2005) begin to include hydrodynamic, magnetic processes and exchange of matter and energy between the disk and halo. They need to be tested.

How do the ISM various phases interact and what are the characteristics of the interfaces at small scale?

Local clouds are inhomogeneous and complex entities (see e.g. Redfield and Linsky, 2008) and we do not know if there is a discontinuity at the clouds outer edges or if their properties gradually merge into adjacent media. Is there a sharp or gradual transition between the Local Interstellar Cloud within which the Solar System is embedded and the G cloud separated by much less than 1 pc? How is the transition with the very tenuous and hot gas of the Cavity? Simulations (e.g. de Avillez & Breitschwerdt, 2005) seem to show that ram pressure is dominating over a wide range of gas temperatures and that motions are typically supersonic. A likely example of a colliding cloud is the velocity difference of 12.7 km/s between the G cloud and another local cloud (Mic), indicating a shock at the interface. This could explain the observed Mic s shape, its higher temperature and large internal turbulence (e.g. Redfield and Linsky, 2008). It has also been demonstrated (Linsky et al. 2008) that the large amplitude scintillation of three quasars can be explained by turbulence where nearby IS clouds interact.

How do cold clouds survive in the hot gas cavities?

In the Local Cavity, cold gas is known to coexist with warm and perhaps hot gas, and with the photoionizing radiation from hot stars like ε CMa. This coexistence is predicted by models (McKee and Ostriker, 1977) if the cold cloud is surrounded by warm clouds that shield the cold gas from external UV and X-ray heating and ionization. All this needs to be further tested, in particular through 3D geometry.

What are the ionization and the depletion in the various phases?

To determine the elemental depletion onto dust grains, one must measure the column densities of all important ionization stages of an element, which is often not feasible. One therefore needs to evaluate the radiation field, which can be tested by the ionization fraction of abundant elements.

What is the nature of stellar-interstellar interfaces?

Similarly to the heliosphere in the Solar System, astrospheres do exist around all stars and the interaction of the IS gas with stellar winds needs to be modeled, and the various mechanisms of feedback to the ISM evaluated. This requires better descriptions of the environments of the stars, and appropriate observations of the physical state in and around the astrospheres.

How much external material is present in the ISM?

One way of testing the hierarchical model of galaxy formation is to look for “alien” material with unusual space motions and abundances. This has been evidenced for the inflow of primordial matter through the study of the IS D/H ratio. However, the study is complicated by the strong depletion of deuterium onto dust grains and the deuterium exchange reactions between the grains and the gas. With CUBES the access to the most refractory species through the Ti II lines and to the detailed line-of-sight structure through the UV neutral sodium line would clarify all D/H previous measurements.

6.9.3 Near-UV lines and galactic ISM three-dimensional mapping

Galactic models of interstellar gas and dust lack precise positioning of the ISM clouds, at a time when those 3D maps are crucial ingredients in the analyses of the Planck and Fermi data. The cloud distribution influences the interstellar radiation field (ISRF) intensity and hardness, and in turn the dust temperature, while the diffuse gamma-ray emission is governed by the cosmic ray propagation through the ISM and up-scattering of the ISRF by cosmic electrons. The galactic ISM, otherwise mapped in an increasingly detailed manner in 2D, should be given its third dimension with much better precision thanks to the forthcoming space mission Gaia, through the positioning of a billion of stars and extinction measurements. A future 3D mapping of the ISM will be also greatly helped by the Gaia-ESO spectroscopic survey (GES), in progress since Jan 2012, and other similar projects.

Near-UV line measurements could greatly enhance the mapping potentialities in two main ways: the 589 nm sodium line primarily detected in the spectroscopic surveys becomes rapidly saturated, which prevents precise measurements (or prevents measurements at all) beyond a given distance, depending on the distance to the galactic plane. The near UV Na I doublet does not suffer from saturation and would give access to large distances. It would also provide the precise line-of-sight velocity structure that would help interpreting other data such like diffuse band absorptions. A survey covering various distances and directions would considerably increase the quality of the 3D mapping. The second strong improvement is the detection of the warm ionized or partially ionized gas phase. While Gaia and GES are able to provide the distribution of the dust (through the reddening) and the distribution of the atomic and molecular

gas (through the Na I or K I lines), the low density ionized ISM will not be probed due to the lack of lines in the spectral regions covered by GES. A high-throughput near-UV spectrograph could bring the complementary strong Ca II H-K lines (393.4 – 396.8 nm), or the Ti II (322.9, 324.3, 338.4 nm). A choice of early-type targets widely distributed in distance and direction would allow inferring the velocity and size distribution of the diffuse clouds, and their dense cloud counterparts would be easily determined by means of radial velocity matching. Exposure times would depend on the distance, roughly exposures shorter than 1 hr would allow improving maps at distances up to several kpc. The combination of all the measurements and radiative transfer models would allow to make invaluable progresses in the determination of the filling factors and interactions between the various phases of the ISM, and to better constrain the interstellar radiation field.

6.9.4 Diffuse interstellar bands

Despite numerous attempts, observations have not allowed yet to solve the longstanding challenge of convincingly identifying the carriers of the diffuse interstellar bands (DIBs). For this reason, new diagnostics and especially the search for weak bands may be vital for progressing. In the visible, no DIBs have been consensually observed short ward of 442.8nm. The spectral region between 300 and 400 nm has not been explored for two reasons: (1) the lack of sensitivity of the spectrographs, and (2) the presence of numerous deep stellar lines that complicate the studies. However the existence of DIBs in this region is not precluded, especially if one considers potential neutral PAHs. Performing a deep search for bands from very small PAHs would potentially lead to important results. The first difficulty is overcome thanks to the high sensitivity of the spectrograph, the second may also be solved for by using well selected targets such as very low-metallicity stars (the GES survey will provide numerous candidates) that have much stellar weaker lines, or by using new fitting techniques based on synthetic spectra that are currently developed and tested. In parallel, measurements of other lines would complement the correlative studies between the DIBs observed by GES and the structure of the IS clouds.

6.9.5 Circumstellar disks and planetary systems around white dwarfs

Contrary to expectations, circumstellar (CS) matter having survived the explosive phase is now known to frequently exist around DAZ/DBZ, but also DAV white dwarfs. Disks of dust have been directly observed in the IR that are attributed to tidally disrupted planetesimals perturbed by asteroids or planets, and a number of stellar metallic lines have been shown to be due to permanent or sporadic infall of circumstellar matter (e.g. Kilic et al, 2011, Farihi et al, 2010a,b). Their observation opens the new exciting way of analyzing the composition of other stellar/circumstellar systems. More recently high ions observed in the UV/FUV have been shown to be of circumstellar origin around a large fraction of stars in a much broader temperature range, very likely due to evaporation of solid material orbiting within the disks (Lallement et al, 2011). Ca II from a gaseous disk has also been very recently detected for the first time towards a DAZ dwarf, and shown to be very likely generated by destruction of asteroids (Debes et al, 2012). With such new potential stars possibly harbouring planetary systems, investigating further the stellar metallic lines (see e.g. Sections 6.2) but also the low-ionization CS gas is an important goal that could also shed light on this unknown phase of the evolution of the disks. A high efficiency spectrograph at high resolution is a perfectly adapted tool for such pioneering observations of white dwarfs, by observing Ca II, but also other potential absorptions by metals at lower wavelengths. In order to separate the photospheric lines from the CS lines and detect the CS contribution high resolution and high S/N (of the order of 100) is mandatory (the first detection was made from a combination of a large number of spectra taken within 4 years, however we are here in a totally new domain of research and only very few objects could be observed, also with much less sensitive instruments). Previous observations of about 10 min exposures with UVES

on such targets in the context of the SPY project led to a S/N of about 15. With the VLT and a spectrograph 2 magnitudes more efficient than UVES one or two exposures of 1 hour should provide a good enough signal for white dwarfs with B<16.5.

Summary of instrument requirements

For the ISM case a wavelength range of 300 – 430 nm is asked for with the Ca II doublet at 393 and 397 nm being among the strongest lines. The analysis requires a spectral resolution of R ≥ 25,000 and typical S/N ratio of at least 50. Overall it is assumed that the analysis of the data is carried out with profile-fitting programs. Otherwise higher resolution such as R~50,000 would be required.

6.10 OH lines (308.5nm) as a tracer of Water in Comets

[Science case kindly provided by Olivier Hainaut (ESO)]

The emission lines of the OH, mainly the 0-0 band (at 308.5nm) and the 1-1 band (at 313.5nm, weaker than the 0-0) of the A ^{2}Sigma$^+$ - Chi ^{2}Pi transition, observed at a resolution of a few thousand, constitutes a powerful diagnostic for the water sublimation in comets (see e.g. Figure 14).

Comets in general:

The OH radical is produced in the coma of comets by photo-dissociation of the water molecules, themselves released from the comet nucleus by sublimation of the water ice constituting a significant fraction of the nucleus, and the bulk of its volatile content (with CO2, CO, CH4, etc). Measuring the OH line at 308.5nm is the only practical way to directly access the water production rate of a comet, and therefore its water content. When that line cannot be measured, the water content has to be estimated by scaling the content of other molecules whose lines are easier to measure (e.g. CN at 388nm, or weaker line of CO+, C2, etc, over the visible spectrum). These scaling factors were accurately measured for some comets since the IUE era. They are of course valid only for objects with a similar volatile content, so in practice these scaling give only very approximate values of the water content. Currently, the OH line is measurable only for very few extremely active comets near the Sun and the Earth, for which the brightness of the line overcomes the poor overall efficiency of the available instruments. A spectrograph with an overall efficiency of ~20% in that wavelength region will open again this field of study.

Main Belt Comets

A specific case of particular interest is that of the Main Belt Comets (MBC). This recently discovered family is constituted of objects whose orbits are dynamically undistinguishable from those of Main Belt Asteroids, but which display cometary features such as a coma and/or a tail. Some of the MBC could unambiguously be interpreted as the result of an impact by a small body, triggering the one-time release of a dust cloud, which disperse and disappear. However, a number of MBCs present genuine cometary features, which strongly suggest that the observed dust is released via traditional cometary activity, i.e. volatile sublimation. Deep spectroscopic observations were performed, but failed to detect any emission line - as expected! Indeed, water is the only volatile material that has a chance to survive in MBCs for more than a few million years (and these objects are believed to have been on their orbits for billions of years). The other volatile ices are completely sublimated away, and cannot contribute to the cometary activity. The only spectroscopic signature of water ice accessible would be that of its product, OH, i.e. the line at 308.5nm (see Figure 14). With the currently available instrumentation, the sensitivity is at best one order of magnitude too low to secure detection.

However, confirming spectroscopically the origin of the MBC's activity would make the Main Belt into a new reservoir of water. Its presence in today's belt would very strongly constraint the dynamical models of formation and evolution of the inner solar system, setting limits to the migration of the planets and on the origin of the various families of asteroids. Moreover, the MBCs would become a very strong candidate to explain the strong excess of water observed on Earth, as transporting icy bodies from the Main Belt is much easier -and therefore more efficient- than transporting them from the Kuiper Belt or the Oort Cloud, the known water reservoir.

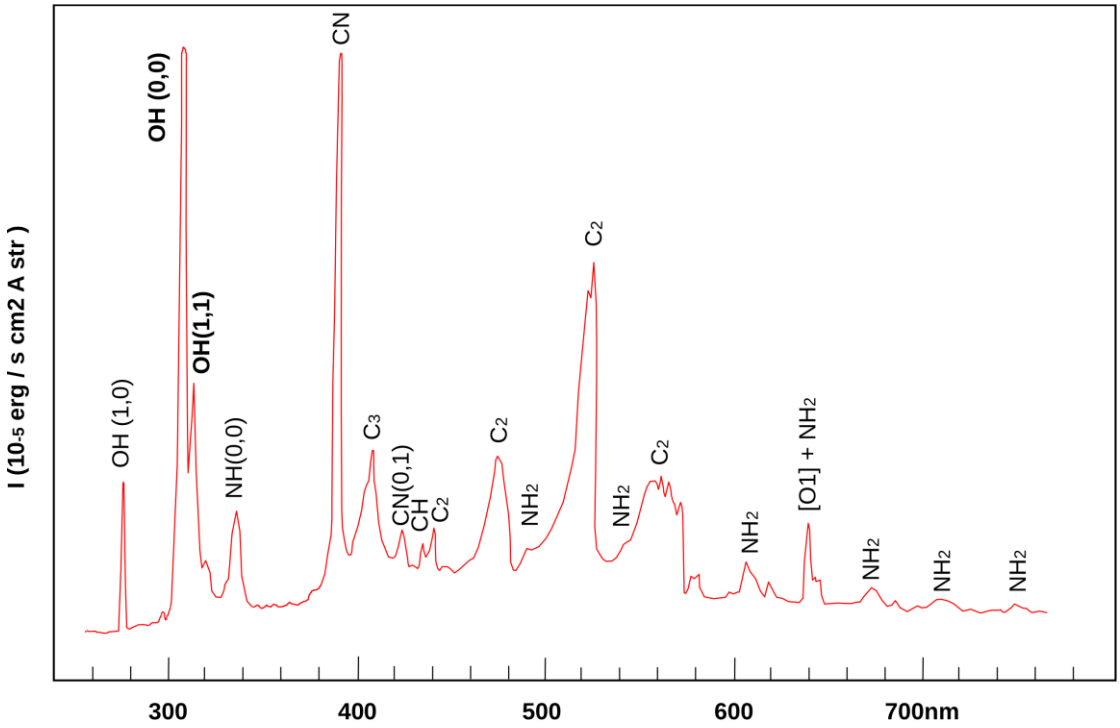

Figure 14: Spectrum of comet 1980XIII Tuttle. The main fluorescence features are indicated. This spectrum is assembled from IUE and ground-based spectra (Larson, priv. comm, fig. adapted from Osborn et al, 1990, Icarus 88, 228). The two lines indicated in boldface are the only ones whose mother molecule is water, and which are observable from ground-based observatories.

Targets and instrument requirements

The V magnitude of comets can cover an enormous range e.g. V = 0 – 20. Typically, interesting targets would be in the V = 10 – 15 range (~solar spectrum). The V mag of the known Main Belt Comets is in the range V = 15 – 20. For the detection of the lines S/N ratios of 5-10 are sufficient, while for quantitative measurements S/N ratios of at least 15-20 are desirable.

The two strongest and also most important emission lines in the UV accessible form the ground are the OH(0,0) and CN lines at 308.5 and 388 nm, respectively. Therefore, a wavelength range covering 305 to 390 nm is required for this science case.

In terms of spectral resolution this case does not set any stringent requirements as long as the main emission lines can be identified. There is an overall preference for maximizing throughput and hence lower spectral resolution compared to e.g. the stellar case.

6.11 General spectral continuum integrity

Current medium- to high-resolution spectrographs often rely on echelle gratings used in high order. These display steep blaze functions that are often difficult to remove to better than 1% and pose a real problem in defining broad features. As an example we show the first three orders of a HARPS spectrum of the metal-poor dwarf star HD 84937 in Figure 15, covering the two Balmer lines H10 and H9.

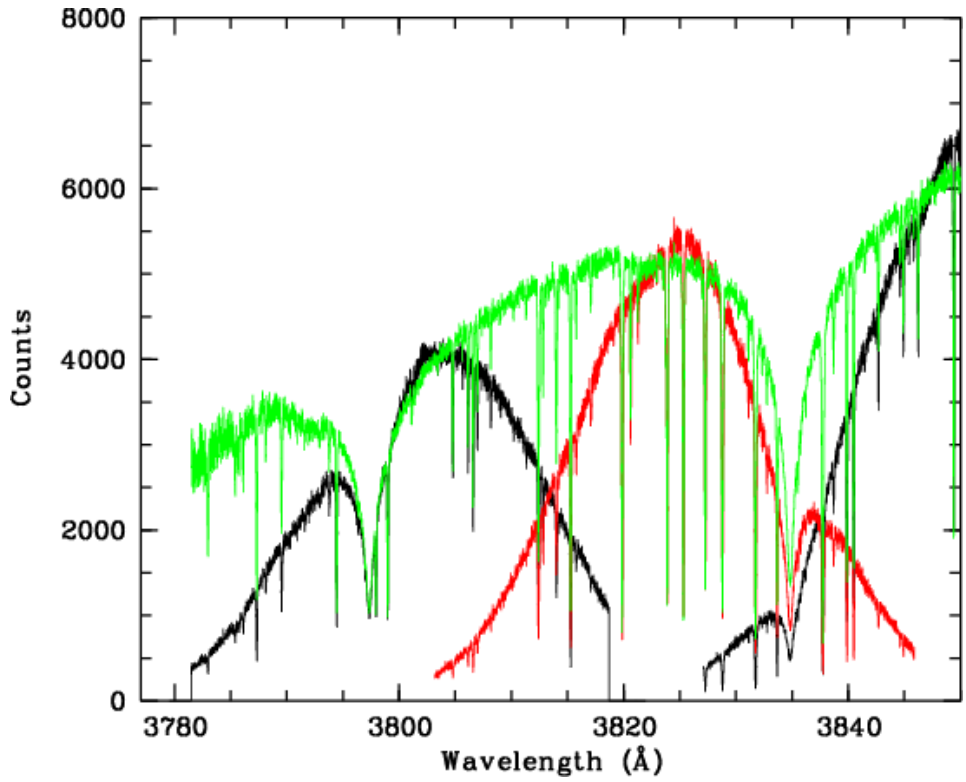

Figure 15: The first three orders (black, red and black) of a HARPS spectrum of HD 84937 prior to blaze correction are shown. The wings of the Blamer lines H10 and H9 cover the whole order. In green the blaze-corrected and merged spectrum is shown. These data have been processed with the ESO HARPS DRS. Although the result may be satisfactory for many purposes it is clear that the wings of Balmer lines have been distorted and artifacts have been created. The most noticeable ones are the depressions at 3790 Å and 3820 Å.

It is possible to appreciate how a precise definition of the wings of the Balmer lines requires a good correction of the blaze profile. We show also the same spectrum, after correction of the blaze function and merging of the orders (green line). Although the HARPS pipeline achieves a good result, it is obvious that the wings of the Balmer lines have been distorted in the process and some artefacts have been created (see also Figure 16). Similar considerations could be done for wide molecular bands, such as NH $A^3\Pi$- $X^3\ \Sigma^-$ at 336 nm.

CUBES will have a substantial advantage with respect to the current echelle spectrographs, since the dispersing element will be a VPH-like grating used in first order. The blaze function will be much less steep and easier to model. Furthermore the wide features will not be split-up into several orders, like they are in echelle spectrographs. CUBES holds the promise of providing us

accurate profiles for wide features, such as Balmer lines (see also Section 6.8) and molecular bands (see also Section 6.3).

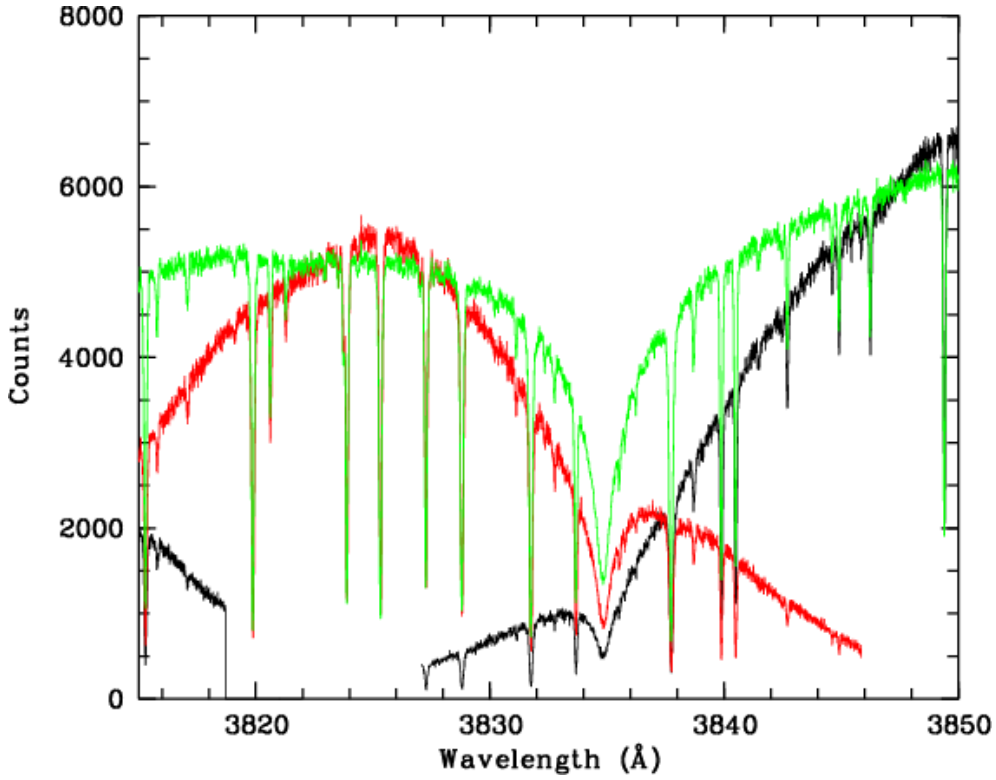

Figure 16: A close-up of the spectrum shown in Figure 15. It is clear that the depression at 3820-3825 Å in the merged spectrum is an artifact of the data processing that prevents us from accurately measuring the red wing of H9.

7 The extragalactic science case

7.1 Introduction

In this chapter we explore the science opportunities for the proposed UV spectrograph for extragalactic targets. Most notably this involves the study of active galactic nuclei (AGN, see Sect. 7.2) and quasar absorption line systems (see Sect. 7.3).

7.2 Active Galactic Nuclei in the UV

[Large contributions to this science case were kindly provided by Giovanni La Mura]

Active Galactic Nuclei (AGN) are characterized by different observational properties. In general, they share very powerful non-stellar energy sources (10^{40} erg s^{-1} ≤ L ≤ 10^{48} erg s^{-1}), emitting their signal over a broad range of frequencies, from radio waves up to X- and γ-rays. When the nuclear source is observed along a nearly unobscured line of sight, it usually dominates the emission, sometimes completely outshining the host galaxy. If, on the contrary, there is severe absorption towards the nucleus, the central source can be obscured, but its influence on the close environment becomes more evident. The former configuration corresponds to what is called a Type 1 object, while the latter is named a Type 2 source, within a spectroscopic classification scheme devised on the basis of the optical-UV observational properties (Osterbrock & Dahari 1983; Antonucci 1993).

A characteristic signature of AGN spectra is the excess of ionizing radiation, associated with the Big Blue Bump, a sharp rise of the SED at a rest frame wavelength λ ≤ 400 nm, which covers the UV domain, probably extending up to soft X-ray energies (Elvis et al. 1994). This feature makes the UV range of AGN naturally interesting. It is directly visible in the spectra of Type 1 sources, while in Type 2 objects its presence can be inferred by the properties of several recombination lines, triggered by the large amount of ionizing photons associated with the bump (Veilleux & Osterbrock 1987; Kewley et al. 2006). Its origin has not yet been fully established, but it is believed to arise from thermal emission in the accretion disk which is feeding on the gravitational field of the central Super Massive Black Hole (SMBH).

AGN spectra in the UV regime are rich in emission lines. The most commonly reported near-UV detections involve bright nebular emission lines from [Ne V] λ342.6nm, [O II] λ372.7,372.9nm, [Ne III] λ386.8nm, as well as some recombination lines of H and He I. However, there are significant differences in the intensity ratios, especially of nebular and recombination lines, among Type 1 and 2 spectra, because of the distinct regions where the bulk of line emission comes from. Some of these lines, especially those of [Ne V] and [O II], act as indicators of the ionization conditions in the line emitting plasma and they can be used to track obscured AGN activity (Heckman 1980; Gilli et al. 2010). Since the currently available spectral coverage of their wavelength range is marginal, most of the work devoted to these spectral features involves objects whose emission lines are brought closer to the optical domain, via cosmological redshift. This is a remarkable concern, because observations at high redshift are typically biased towards the brightest sources. Therefore, a comparison with the properties of local objects becomes fundamental to account for possible selection effects and cosmic evolution.

Besides the spectral features mentioned above, the near-UV window includes several contributions of great importance for the investigation of AGN. In the low redshift domain, the limit of the hydrogen Balmer series falls in this wavelength range, while, looking at higher redshift objects, broad emission and absorption features, strictly connected to the nature of the

unresolved nuclear source, enter the near-UV frequencies. In order to point out the contributions resulting from the analysis of these properties, it is convenient to discuss them according to their different origin.

7.2.1 The Narrow Line Region

The emission lines that we commonly observe in AGN spectra can be classified in two categories: broad lines, with FWHM≥10^3 km s^{-1}, and narrow lines, with FWHM≤10^3 km s^{-1}. They originate from two distinct regions, characterized by different physical properties. The Narrow Line Region (NLR) is filled by a tenuous plasma (10^3 cm^{-3} ≤ N_e ≤ 10^4 cm^{-3}), ionized by the energetic output of the AGN central engine, through a combination of photo-ionization and shock processes, whose signature is left in diagnostic emission lines, such as [Ne V] λ342.6nm, [O II] λ372.7,372.9nm, [Ne III] λ386.9nm, Hβ, [O III] λ495.9,500.7nm, [N II] λ654.8,658.3nm, Hα, and [S II] λ6716,6731 (Solórzano-Iñarrea et al. 2001). In nearby objects the NLR can be resolved and it is often observed to have a conical, or bi-conical morphology, with an axis of symmetry which, in the case of strong radio emission, lies along the direction of the radio axis (Haniff et al. 1988; Pogge 1989; Wilson & Tsvetanov 1994).

The main property, which distinguishes the NLR gas from other nebular environments, such as planetary nebulae, is the source of ionization, that involves a different radiation field, with respect to the case of a hot star, and some contribution from shock fronts (Moy et al. 2002). The result is that NLR spectra may exhibit a wide range of relative line intensities, reflecting the role played by the various ionizing factors (Radovich et al. 1998). Indeed, investigating the properties of nebular environments is one of the most successful fields of astrophysical spectroscopy and the NLR of active galaxies represents an attractive target. The relative strengths of emission lines originated by a single element in different ionization configurations, not frequent in the optical domain, but available in near-UV for [Ne V] and [Ne III], are sensitive to the source of gas ionization, and they can be used to distinguish among radiation and shock processes. Resolving the profiles of these emission lines and combining them with observations of other species, such as [O II], provides further details concerning the gas kinematical and chemical configuration, which are crucial to understand the origin of the NLR gas and its role within the host galaxy. The contribution of a spectrograph with optimized near-UV sensitivity and resolution R ~ 20,000 will shed new light on the properties of the NLR in a large number of sources.

7.2.2 The Broad Line Region

In contrast to the narrow emission lines, the broad lines appear exclusively in Type 1 AGN spectra and they are not generally found in correspondence with forbidden atomic transitions. Some exceptions are possible in the profiles of the brightest features, such as [O III] λ495.9,500.7nm. The most prominent broad emission lines include Lyα λ121.6nm, C IV λ154.9nm, C III] λ190.9nm, Mg II λ279.8nm, the Fe II multiplets, He II λ468.6nm, He I λ587.6nm, and the Balmer, Paschen, and Brackett series of H, in the optical and IR wavelength ranges. In several cases, the far UV lines, especially Lyα, as well as the lines from C IV, C III], and Mg II, are strong enough to be clearly detectable in high redshift objects, where they are observed at near UV-optical frequencies. However, the observation of these lines in the optical domain implies the exploration of redshifts in the range of 0.6 ≤ z ≤ 2.7, where intrinsic source brightness selection effects are certainly significant. Studying these lines in the near-UV regime allows us to explore considerably closer sources (z = 0.25 is high enough to observe Mg II, while 0.83 ≤ z ≤ 1.88 is still needed to detect the C and Ly spectral features), with clear advantages both in terms of selection efficiency and in the understanding of the object evolution through different cosmological epochs. Indeed, these UV lines, together with Hβ in the optical domain, provide the best established

tracers of the dynamical effects arising from the SMBH gravitational field (Kollmeier et al. 2006; Vestergaard 2002; Vestergaard & Peterson 2006).

Several arguments confirm a strong interaction between the continuum source and the BLR (Blandford & McKee 1982; Wandel et al. 1999). Moreover, the detection of Type 1 spectral features in the polarized signal of some Seyfert 2 galaxies reveals the existence of an intrinsically Type 1 spectrum, reflected onto the observational line of sight by a directly illuminated medium, located away from the obscuring material that surrounds the nucleus (Antonucci & Miller 1985). The BLR unresolvable structure, however, places severe uncertainties on the determination of the central engine physical properties from the analysis of the emission lines. It is worth recalling that we have only marginal knowledge of the actual ionizing radiation SED and of its influence on the line emission process (Elvis et al. 1994; Mullaney & Ward 2008), this is among the main problems that need to be solved. Furthermore, some heavy ions, especially Fe II, are contributing to the optical-UV bands with complex line multiplets, which require a spectral resolution of $R \geq 15{,}000$, in order to clarify their origin. It is estimated that Fe II emission line multiplets can account for a significant fraction of the total energy processed in the BLR plasma (up to $\sim 50\%$, Joly 1987) and they are part of the strongest relationship existing among the spectral properties of different Type 1 AGN (Boroson & Green 1992). Fe II multiplets are found from the far UV regime all the way down to optical frequencies (Baldwin et al. 2004), but their properties in the near UV still have to be thoroughly explored. The case for a complete understanding of this important contribution to the BLR spectrum is further stressed by the circumstance that such an ion cannot survive direct exposure to the AGN radiation field. Its presence constrains the BLR self-shielding capability, which is a fundamental tool to penetrate the structure and dynamics of matter within the innermost core of AGN (Ferland et al. 2009). Therefore, a new scientific instrument with $R \sim 20{,}000$, appropriately devised to analyze the near UV regime, would play a major role in further developing these topics.

7.2.3 AGN circum-nuclear environment

It is often observed that the circum-nuclear regions of active galaxies, within a distance $r \approx 1$ kpc from the AGN, have significantly different properties, with respect to quiescent systems. Several investigations have found evidence of young stellar populations, indicating that relatively recent star formation activity occurred in the nuclear regions of active galaxies (González Delgado et al. 2001; Rafanelli et al. 2009).

Analysis of the near-UV regime at a spectral resolution $R \sim 20{,}000$ becomes particularly attractive in the case of the circum-nuclear regions of nearby low luminosity AGN and Seyfert 2 galaxies (Cid Fernandes 2001a, 2001b). It has been pointed out that the stellar populations of these objects share an excess of intermediate-age stars. The existence of absorption features, corresponding to the high-order Balmer lines, and the shape of the Balmer and two-photon continuum constrain their recent star formation history. The signature of recent star formation is statistically relevant even in relatively low spatial resolution observations ($\sim 1'' - 3''$), but bringing together better spectral and spatial resolution capabilities represents a fundamental goal. Indeed, in lower resolution spectra ($R \leq 10{,}000$) it is very difficult to assess the presence of blended absorption and emission lines. For this reason, the comparative study of spectral line profiles of nebular and permitted lines will reveal precious details on the distribution of the stellar and gaseous components surrounding the nucleus and on their reciprocal interplay.

7.2.4 Absorption systems

In spite of the dominant role played by emission line plasmas in the spectra of AGN, several absorption features bring a relevant contribution to our understanding of the underlying physics. The strongest absorption lines are associated with the resonance transitions of the most common

ions and, since they involve the fundamental levels of the electron configuration, they typically fall in the far-UV regime. It is estimated that a fraction of approximately 10% of QSOs exhibit broad absorption lines, most often associated with UV lines of the BLR spectrum, such as Lyα λ121.6nm and C IV λ154.9nm. Their systematic blueshift, with respect to the local rest frame, suggests an origin in outflowing winds covering a small range of inclinations, on the border of the obscuring structure which distinguishes among Type 1 and Type 2 objects. Spectropolarimetric observations support this picture, detecting on average a larger degree of polarization in the continuum and, above all, in the absorption troughs of broad absorption line sources, with respect to normal Type 1 objects, pointing towards an enhanced contribution from light scattering in the resulting spectrum (Schmidt & Hines 1999; Ogle et al. 1999). Since a spectral resolution of R ~ 20,000 is fundamental to probe the kinematical configuration of the absorbing material, the optimized near-UV sensibility offered by the proposed spectrograph would significantly increase the number of sources where such observations can be carried out.

7.2.5 Instrument requirements

Most of the above considerations apply to physical environments whose size is below the order of 1kpc (approximately the length subtended under 1" at a redshift $z = 0.05$). Since AGN are sharply distinguished from the background, the instrument field of view is not a critical issue. Good performance, on the other hand, is required for spectral resolution and coverage, in order to provide detailed profile information in the available spectral features and possibly resolve the multiple line systems.

Although radiation polarization is not a general characteristic of AGN emission, spectropolarimetric capabilities should be considered. The BL Lac and Optically Violent Variable (OVV) objects are characterized by appreciable fractions of polarized flux (~ 1−5%) in the continuum. When detected, the degree of polarization increases with frequency and it peaks in the broad absorption troughs seen in some QSOs. The polarization orientation, however, changes with the spectral components due to its different origin. Polarization induced by reflection components, mainly affecting broad emission and absorption systems, has already been discussed. In the case of the continuum light, instead, it is believed to descend directly from the radiation source, when it includes a non-thermal contribution from a jet of relativistic particles. Polarized flux in the near-UV window, therefore, is a valuable tool to identify reflected components, that can originate from the BLR, and to investigate the spectral properties of jet related emission.

A typical S/N ~ 50 over the spectral range covered is required to address the scientific issues that were previously outlined. If we consider targets with a magnitude of $V_{mag} = 16$ and spectra like those illustrated in Figure 17, this requirement is achieved with exposure times ranging from t ~ 3600 s for a Type 1 target up to t ~ 10800 s for a LINER class object. Increasing the exposure times (up to t ~ 10 h), equally good S/N ratios can be achieved down to $V_{mag} = 16.5$ for LINER targets and to $V_{mag} = 18$ for Seyfert 1 and Seyfert 2 galaxies, while QSOs might be observed at even fainter magnitudes, because of their stronger UV excess. Table 1 provides a schematic overview of the number of sources within such limits and of their redshift ranges. The main instrument requirements based on the AGN science cases can be summarised as follows:

- Focus on optimizing UV throughput
- Spatial resolution α≈0.8" (seeing limited)
- Spectral resolution $15{,}000 \leq R \leq 30{,}000$
- Spectral coverage from 300nm to 400nm

7.2.6 Target considerations

Analysis of the existing catalogues of extra-Galactic sources reveals that the number of possible targets to be studied with a near-UV spectrograph is remarkably large. Considering only objects that are brighter than $V_{mag} = 16$ (the limiting value for which S/N lies above 50 throughout the whole spectral range in $t \sim 1$ h exposure time), more than 1300 AGN are known, with a declination $\delta < 20^{\circ}$. Beyond $V_{mag} = 16$, the number of targets increases steeply. Figure 18 illustrates the distribution of targets for which spectra with S/N ≥ 50 over the whole spectral window can be observed. It also provides a comparison of instrument performances, based on a preliminary exposure time calculator (ETC), showing the improvements that the proposed spectrograph would offer with respect to VLT UVES and X-shooter, the only spectrographs covering the near-UV window with medium to high spectral resolution currently at ESO VLT. The results clearly show that the proposed spectrograph performances represent a significant improvement with respect to UVES, especially at the shortest wavelengths. Although X-shooter might achieve comparable performances when gains from the lower spectral resolution are taken into account, its spectral resolution is far too low (R = 5,100; 1" slit) for the proposed science cases and the associated spectral response varies with wavelength ("echelle orders"). Therefore, the proposed spectrograph would reach limits where a large population of targets lies, thus probing objects whose characteristics are extremely rare in brighter magnitude-limited samples.

Table 1: Target properties

Class	# Targets	z_{min}	z_{max}	V_{min}	V_{max}
Seyfert 1	206	0.001	0.240	12.72	18.00
Intermediate	1382	0.003	0.268	11.79	18.00
Seyfert 2	717	0.001	0.270	9.04	18.00
LINER	390	0.001	0.141	9.25	16.50
QSO	3743	0.016	4.545	10.16	18.00
BL Lac	109	0.023	1.72	12.81	18.00
Unclassified	376	0.001	0.127	10.83	16.50

Notes: Distribution of known AGN with $\delta < 20^{\circ}$ and magnitude brighter than the estimated limit for high S/N spectroscopy. The target properties are based on the latest edition of the Catalogue of Quasars and Active Galactic Nuclei (Véron-Cetty & Véron 2010).

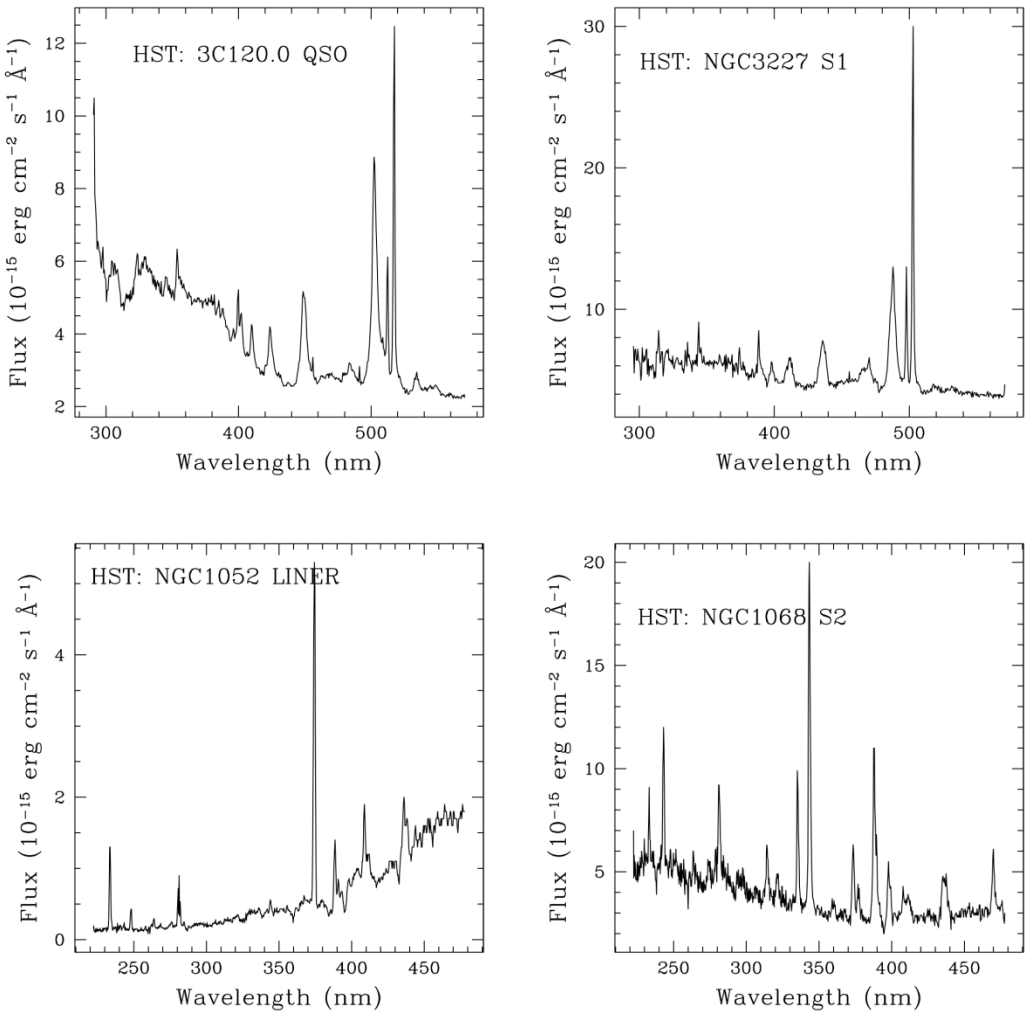

Figure 17: Prototype input spectra used in the preliminary exposure time calculations for the QSO, Seyfert 1, Seyfert 2, and LINER object classes.

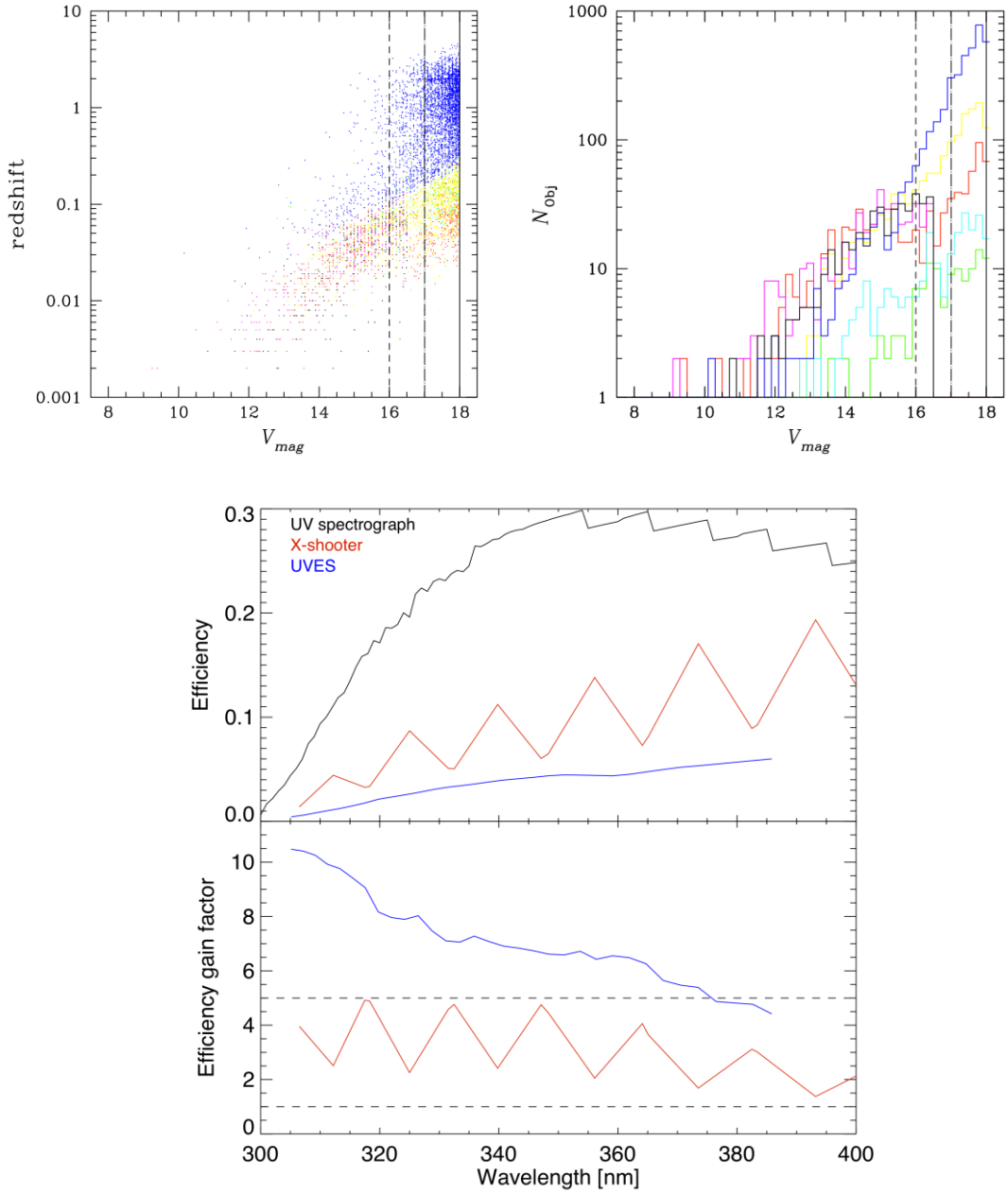

Figure 18: (**Upper left**) Redshift vs. magnitude distribution of targets. (**Upper right**) Histogram of targets for which high S/N spectra can be extracted. Vertical lines correspond to 1 h (dashed line) and 10 hr (continuous line) exposures. The dot-dashed line shows where S/N lies above 50 down to λ = 320 nm in a 10 h exposure of a QSO spectrum with UVES. QSO are represented in blue, BL Lac objects in green, Seyfert 1 in cyan, intermediate Seyferts in yellow, Seyfert 2 in red, LINER in magenta, and unclassified sources in black. (**Bottom**) Instrument efficiency including atmospheric transmission and efficiency gain factor vs. wavelength. The black line stands for the proposed UV spectrograph, red for X-shooter, and blue for UVES. Note, that the wavelength range of ESPRESSO starts only at 380 nm. Different spectral resolutions between the instruments are not taken into account in this plot.

7.3 Quasar absorption line systems

The blue end of the optical wavelength range is of utmost importance for the study of:

i. the intergalactic medium at intermediate redshifts (z∼1.5−2), its physical state (temperature, ionization) but also its metal content (through O VI), and

ii. the interstellar medium of high redshift galaxies and in particular its molecular content (H_2 for z>2; CO for z>1).

High spectral resolution is needed not only to decompose the absorption profiles but also to derive accurate characteristics of the absorption lines (column density and Doppler parameter). A resolution of R∼20,000 associated with very high-efficiency below 400 nm is a good compromise between this necessity and the need to target fainter quasars compared to what is possible to achieve with available high resolution spectrographs and in particular UVES.

Specific projects include: (i) the determination of the ionizing background and the physical state of the IGM by analysing the characteristics of the Lyman-α forest and interpreting the proximity effect; (ii) the determination of the metal content of the IGM; (iii) the study of the small-scale transverse correlation in the IGM by observing pairs of quasars with small separation in the sky; (iv) the study of the galaxy-IGM interaction by determining the correlation between the properties of galaxies and the associated gas seen in absorption; (v) the detection and characterization of the long-sought cold diffuse molecular component of the interstellar medium (ISM) of high redshift galaxies.

7.3.1 The intergalactic medium at z = 1.5−2

Numerical *N*-body simulations have been successful at reproducing the observed characteristics of the Lyman-α forest corresponding to the absorption signature of the intergalactic medium in QSO spectra. The gas traces the potential wells of the dark matter and its large-scale structures. The IGM is therefore seen as a smooth pervasive medium which is the reservoir of baryons for galaxy formation. In turn, because of feedback processes, galaxy formation is imprinted on the properties of the IGM.

7.3.1.1 Evolution of the IGM

The properties of the IGM have been well studied at redshift larger than z∼2 thanks to the numerous data obtained with UVES on the VLT (e.g. Bergeron et al. 2004, The Messenger, 118, 40) and HIRES on Keck. However, it has been shown recently that the data acquired up to date are not enough to definitely tackle important questions such as what is the temperature evolution of the IGM and how is it related to the reionization of the Universe (Bolton et al. 2010, Becker et al. 2011). A spectrograph very efficient in the blue and with R∼10,000-20,000 would be most important to extend the properties of the IGM down to z∼1.5 and to increase the statistics. X-shooter is of too low resolution to resolve the Jeans length and UVES is time consuming due to the limited throughput.

7.3.1.2 The ionizing background at z=1.5−2

It is well known that the characteristics of the Lyman-α forest change in the vicinity of the quasar due to the additional ionizing flux emitted by the quasar itself. The mean neutral hydrogen fraction decreases when approaching the quasar. It is possible to use this effect, together with knowledge of the quasar luminosity and its position, to derive the mean flux of the UV background. In this way, it is possible to probe the presence of overdensities associated with the quasar (Guimaraes et al. 2007). Using pairs of quasars would allow investigating the transverse proximity effect.

7.3.1.3 Metals in the IGM

With the advent of UVES, it was realized that the IGM contains a fairly large amount of metals, revealed in particular by C IV and O VI absorptions. The O VI transitions at 103.1 and 103.7 nm are redshifted in the very blue part of the optical spectrum for $z > 2$. The properties of these metals and their spatial location are barely understood because C IV and O VI do not seem to follow each other well and there seems to be a large fraction of IGM absorbers with large oxygen abundances (Schaye et al. 2003, Muzahid et al. 2012). The origin of this pollution by stars is therefore unclear (Pop III objects or winds from primordial galaxies). Here, R ~ 20,000 and again high sensitivity in the blue are well suited.

7.3.1.4 Spatial structure

Recently, pairs of quasars with small separation in the sky have been observed with FORS and UVES to derive the transverse correlation function of the IGM on small scales (Coppolani et al. 2008; Capetta et al. 2010). Low resolution is enough to probe the overall correlation function and X-shooter will be the most efficient instrument to improve these measurements in the near future (FORS has very low efficiency in the blue). Higher spectral resolution is needed, however, to derive the velocity and density gradients in the IGM in order to understand how the gas is flowing towards the high-density regions. The resolution of UVES is too high for this problem and it would be limited to only the brightest. The sensitivity of the proposed spectrograph, combined with its appropriate spectral resolution, will undoubtedly boost this field once adequate new pairs of quasars (matched in redshift and magnitude) are discovered by the ongoing surveys (e.g. BOSS).

7.3.2 The galaxy-IGM interaction

The interplay between galaxies and the IGM is a key element in understanding galaxy formation. The IGM is the reservoir of baryons for galaxy formation and galaxies accrete warm gas from the IGM along the filaments of large-scale structures. In turn, feedback processes that return energy and material back to the IGM from the galaxy population are needed to explain the colours and the luminosity function of present-day galaxies (Bower et al. 2006). Indeed, winds from star-forming galaxies have been detected (Adelberger et al. 2003).

These processes can be explored by studying the correlation between galaxies (or quasars for the transverse proximity effect) and the absorptions detected along QSO lines of sight in the same field. These issues can also be investigated by observing quasar lines of sight in fields where galaxies have been surveyed. In particular it would be very interesting to correlate the metal absorption lines with the positions of the galaxies (see Scannapieco et al. 2006).

At large redshift ($z > 2.5$), there is an excess of H I absorption compared to the mean within ~5 Mpc of a typical L* Lyman break galaxy. It is however unclear whether this excess holds up to the galaxy itself or if there is less H I absorption close to the galaxy (<1 Mpc) due to the effect of feedback (Crighton et al. 2011; Rudie et al. 2012). For these galaxies, it would be most interesting to search for associated O VI absorption that could reveal galactic winds. In addition, these studies could be extended to redshifts corresponding to the peak of the star formation activity in the universe.

The proposed spectrograph is a very interesting instrument for these issues because it would allow the study of these effects at lower redshift and the detection of O VI in Lyman break galaxies. Most importantly fainter quasars (compared to UVES) can be targeted in the few deep fields where a tremendous amount of information is already available. The resolution of X-shooter is again here not high enough. A resolution of at least R~15,000 is required to reveal the spatial

distribution of the gas along the line of sight at these scales. A resolution of R~20,000 is therefore well adapted.

7.3.3 The interstellar medium of high-*z* galaxies

Although molecular hydrogen is a prominent constituent of the interstellar medium in galaxies, it is rarely detected directly. In emission, only excited H_2 is detected and only absorption can allow us to derive physical properties of the standard diffuse molecular medium. The first systematic search for molecular hydrogen in high-redshift (z_{abs} > 1.8) DLA galaxies was carried out using UVES at the VLT (Noterdaeme et al. 2008) and discovered 13 H_2 systems (see also Figure 19).

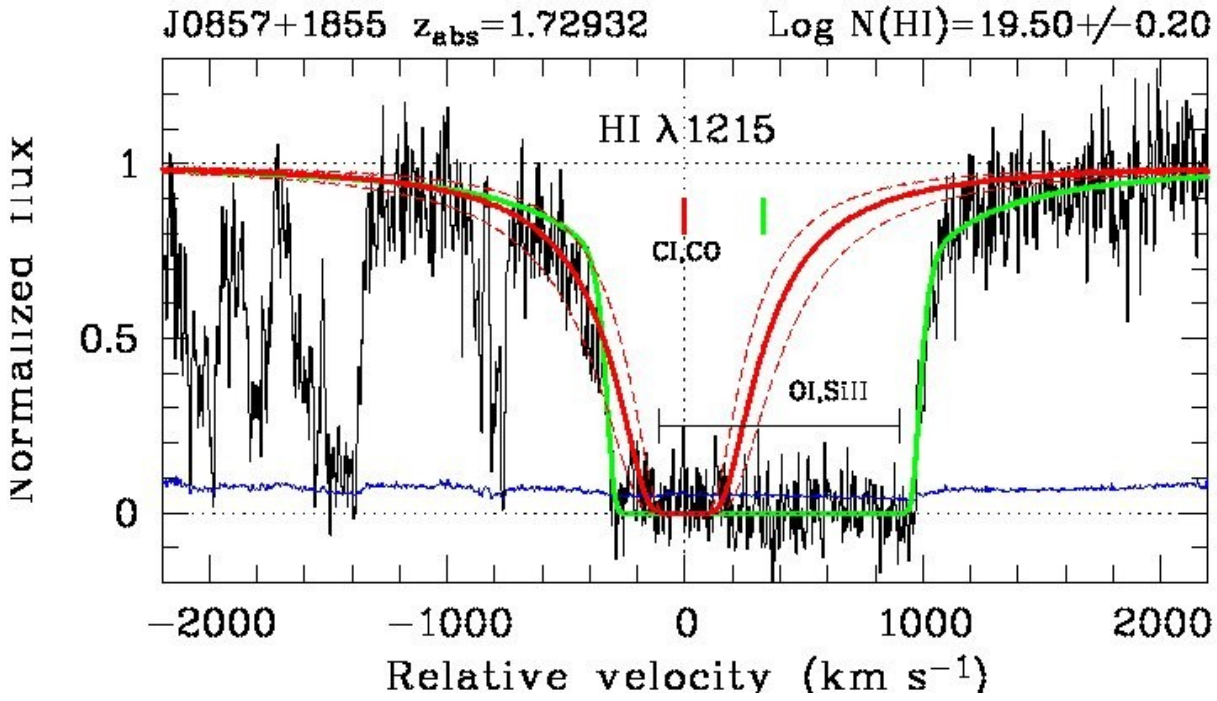

Figure 19: Example of HI profile observed at 330nm. The blue component has H_2 and CO absorption associated. It can be seen that SNR~10 and R~15000 is required for such decompositions (source: P. Petitjean).

Using refined selection criteria including the results of this survey and the use of C I absorption, it is possible to increase the efficiency of the selection of H_2 bearing systems to about 30%. Applying these criteria to the SDSS database yields a sample of candidates for the detection of molecules. H_2 is now routinely detected although the number of systems that can be observed is limited by the sensitivity of the instrument. In addition CO has been discovered together with several HD absorbers (Srianand et al. 2008). These detections open up the exciting possibility to study astro-chemistry at high redshift. CO is also a thermometer for the CMB temperature (see Figure 20)

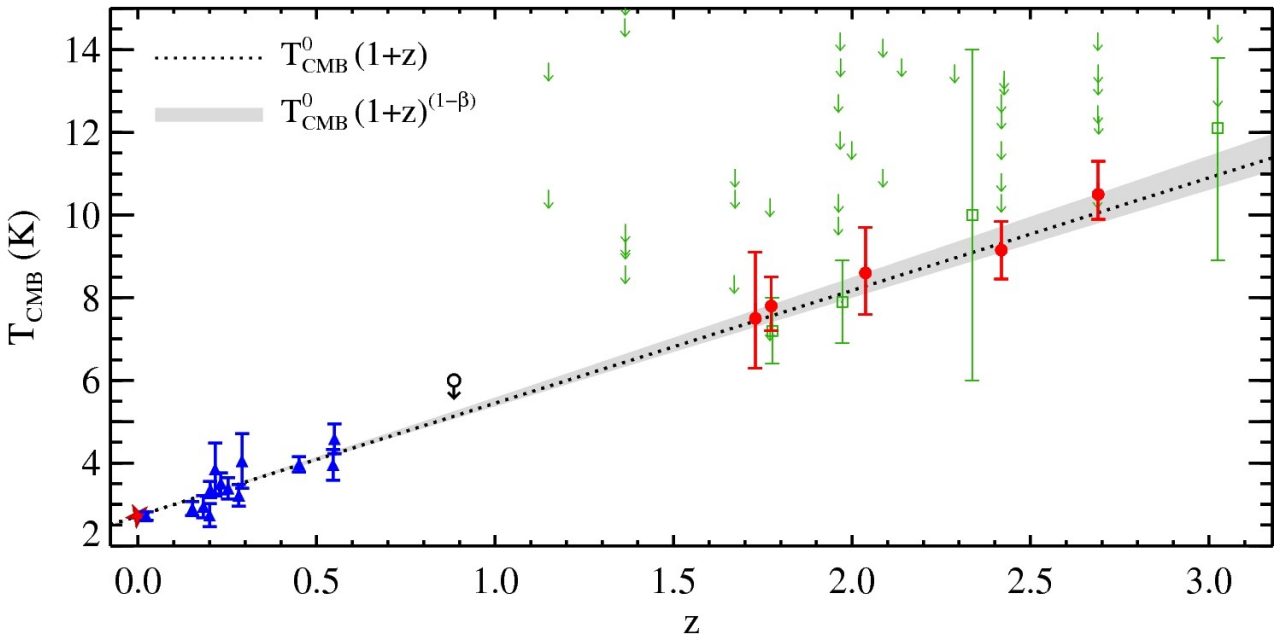

Figure 20: Measurement of the temperature of the CMB at high z using the excitation of CO by the black body radiation.This is a direct test of the BB theory (Noterdaeme et al. 2011).

With UVES we are just investigating the top of the iceberg. H_2 transitions are found deep in the blue and the proposed spectrograph can be considered as the ideal instrument to study the diffuse molecular ISM at high redshift because of both the sensitivity and the resolution. It will be possible to go fainter and to hit the bulk of the population.

7.3.4 Target considerations

In total, the SDSS-BOSS project (first release DR9 is due in July 2012) will provide 160,000 QSOs at z>2, a third being observable from VLT. The median magnitude is roughly 1 mag fainter than for DR7; thus DR9 will provide at least three times more targets than DR7. The typical target will be a point source of g=20.5 and a signal-to-noise ratio (SNR) ≥10 for λ > 330nm is required for the proposed science. The QSO absorption line studies benefit from being able to reach the faintest targets possible hence it is important to optimize the spectrograph with this in mind.

7.3.5 Instrument requirements

For the quasar absorption line system studies an increased wavelength range translates in a direct increase in science potential. A goal would be to cover the length of the Lyα forest, which translates into a requirement of minimum spectral coverage of about 80nm with a goal of 100nm.

There are no strict drivers for absolute starting and end wavelengths since targets can always be chosen at the appropriate redshifts. In order to achieve the required SNR even for the faintest targets it would be advisable to match the instrument wavelength range to the high throughput region, e.g. 320 – 400nm (see Figure 18).

In terms of spectral resolution the “Galaxy-IGM interaction” case (Section 7.3.2) sets a minimum requirement of R~15,000 even so other science cases could be carried out down to about R~10,000. To be able to use slightly lower resolution is an advantage as it offers the possibility to

reach fainter targets. Together with the availability of the 160,000 z>2, g<22 BOSS quasars in 2014, this will open a new window for the study of the interstellar gas in high redshift galaxies.

Reasonable SNR (~10) even for the faintest targets is of importance to this science case therefore the spectrograph and operational concept must allow for the possibility of long exposures (i.e. 45min exposure time) and the possibility to co-add several (e.g. 10) exposures. In order to avoid degradation of spectral resolution and optimisation of the SNR the stability of the spectrograph should be better than 1/5 pixel in wavelength direction and better than ½ pixel in cross-dispersion direction (including atmospheric dispersion effects).

Using the preliminary ETC with the following setup (point source, QSO template at z=1.5, V=20.5, airmass=1.3, slit transmission=82%) a SNR ~ 10 for λ>330nm can be achieved in 4x45min. Given the low flux rate from the target and sky per DIT and reference area (104 e-/DIT and 32 e-/DIT, respectively) we derive requirement for RON <= 3 e-/pixel/DIT and reasonably low dark current rate <0.001 e-/pix/s.

8 Instrument competitiveness

The proposed UV spectrograph, as any new VLT instrument, should be able to maintain and expand the La Silla Paranal Observatory world-wide competitiveness in the years following ~2015. As such, it should not only be superior to existing instruments in terms of performance, but should also extend the scientific capabilities of the observatory into unique areas. In this section we assess the instruments competitiveness by comparison with existing and planned facilities.

8.1 Competition within ESO

Currently operational spectrographs with medium to high spectral resolution and UV wavelength coverage include X-shooter and UVES at UT2. Both instruments are cross dispersed thus offering a large wavelength coverage across the optical regime but are not optimized towards the UV. A comparison of efficiency estimates between the proposed spectrograph and the existing facilities is given in Figure 18. Compared to UVES, which can provide the same or better spectral resolution, the proposed spectrograph offers access to targets up to 3 magnitudes (at the atmospheric cutoff) fainter than currently possible. Also with respect to X-shooter the proposed spectrograph is significantly (up to 5 times) more efficient. But more importantly X-shooter cannot provide the required minimum spectral resolution to resolve important UV lines (e.g. Be II lines; R ~ 20,000; see Figure 6). From the above considerations we conclude that the proposed spectrograph accesses a new parameter space in the efficiency versus spectral resolution plane.

Among the new instruments to be built for the VLT or La Silla only ESPRESSO is relevant in the context of the proposed UV spectrograph. In terms of parameter space the two instruments are well separated since ESPRESSO does not cover wavelengths below 380 nm at all. In fact, a potential overlap region from 380 to 400 nm could be used for cross-calibration purposes with ESPRESSO living up to much more stringent stability criteria. Also scientifically, ESPRESSO offers rather *cooperation* than *competition*, for example, in the stellar science case. Basic stellar parameters, such as metallicity or abundance ratios (e.g. [Mg/Fe]) are more efficiently determined with a long wavelength range such as the one offered by ESPRESSO, whereas more specific science questions outlined in the UV stellar science case (see Section 6) can only be done with a spectrograph covering the UV. The combination of both spectrographs, available at the same observatory, offers a unique facility for a broad range of chemical abundance studies of stars.

Needless to say that the E-ELT will be optimized towards optical and (near) IR wavelengths and thus does not target the UV (λ<370 nm).

8.2 World-Wide competition

Making use of publicly available information on existing as well as planned ground- and space-based facilities around the world, we compiled the following summary of competitors for the proposed UV spectrograph. Among the space-based missions we note some which can provide potential targets rather than posing a competition for the proposed UV spectrograph.

8.2.1 Ground-based

Similarly to UVES, the high-resolution spectrographs HIRES (Keck) and HDS (Subaru) provide, due to their optimization for large wavelength coverage and high spectral resolution, limited throughput in the UV. The proposed UV spectrograph will outperform them by a factor of several.

An UV efficient instrument is the prime focus Robert-Stobie-Spectrograph at SALT (http://www.sal.wisc.edu/PFIS). Commissioning started in 2011 and it is currently available at shared risk. The instrument takes advantage of the blue-optimised telescope and covers the

range 320−1000 nm with a throughput of 25% in the UV. However, its spectral resolution is below R ~ 10,000 and therefore not suited to most of the science case presented in this document.

At Gemini, three conceptual design studies for a high-resolution spectrograph (dubbed "GHOS"; R ~ 40,000) are being conducted with a nominal wavelength range of 370−1000 nm and a goal of 300−1100 nm. The outcome of the study and the associated delivery schedule is presently unknown.

8.2.2 Space-based:

Perhaps the most prominent spectral UV coverage above the atmosphere is provided by the Hubble Space Telescope (HST) with the Space Telescope Imaging Spectrograph (STIS) and the Cosmic Origins Spectrograph (COS). The competition for the proposed UV spectrograph is limited since COS aims at wavelength shortwards of 300 nm and STIS provides only a spectral resolution of R ~ 6,000 for 300−400 nm. Furthermore, HST is getting close to the end of its lifetime and is therefore unlikely to be operational beyond 2015.

The World Space Observatory-Ultraviolet (WSO-UV) is a project by the Russian Space agency (http://wso.inasan.ru) with important contributions from Germany and Spain. A 1.7 m mirror will feed a high resolution (R ~ 50,000) double echelle spectrograph (103−310 nm) and an Imaging and slitless spectrograph (115−700 nm). The telescope is scheduled for launch in 2016 and will be operated in a way similar to HST although details remain sketchy at this point. Due to technical advances in UV detectors the echelle spectrographs are expected to clearly outperform STIS. The wavelength ranges of WSO-UV high-resolution spectrographs and CUBES will be exactly complimentary and thus could again form a very successful cooperation just like HIRES on Keck and UVES on the VLT did with HST spectrographs.

Although the GALEX satellite has been turned off Dec 31st, 2011 and was aimed at wavelengths shortwards of 300 nm, its archive provides a noteworthy source of targets for the proposed UV spectrograph. Its imaging surveys (spatial resolution few arcsec) covered a large fraction of the sky and a final data release, publicly available through MAST (http://archive.stsci.edu), will be done following a close-out calibration effort.

India is planning to launch the multi-wavelength astronomical observatory ASTROSAT (http://www.iucaa.ernet.in/~astrosat) late in 2012. Equipped with two 40 cm telescopes it provides imaging (130−320 nm) at 1.8 arcsec resolution and very limited spectral (filters) capabilities.

NASA's plans on a next generation UVOIR space telescope (ATLAST; Postman 2009) circled around 8-16 m class telescopes with superb spatial resolution. While originally targeted for a launch around 2020, such plans could only be realized, given the current funding situation, well beyond the time frame under consideration for the proposed UV spectrograph.

8.3 Conclusion

In summary, we find that in the timeframe 2017 to 2022, the proposed UV spectrograph would be a unique facility at the VLT given its high throughput at medium spectral resolution (R ~ 20,000). Important synergies with ESPRESSO and e.g. the World Space Observatory-Ultraviolet could be realized for at least the first 5 years of operation.

9 Science Requirements

This section summarizes the science requirements derived from the science cases presented in this document. A certain level of judgment is applied to arrive at realistic constraints for the proposed UV spectrograph.

9.1 Observing modes

All science cases presented in this document can be suitably covered with one basic spectroscopic observing mode where the target is placed on the centre of a slit. The stellar cases, by definition, are limited to point sources and also the other cases are largely restricted to objects with little spatial extent. To enable sky subtraction a long-slit (slit length ≥10") design seems appropriate. Sub-modes shall include the provision of more than one spectral resolution setting – see Section 9.2.

Summary

- One main spectroscopy mode, which allows obtaining the UV spectrum of targets discussed in this science case.

Note, that the instrument will need to provide more technical modes allowing for e.g. target acquisition, calibration and maintenance.

Overall the science case provides a large range in programs without the clear identification of an overriding topic. This implies that CUBES will likely be used by many different users with programs limited in duration (typically a few hours up to ~3 nights).

9.2 Wavelength range and spectral resolution

The overall wavelength coverage is targeted at the UV which is, for ground based instruments, bound by the atmospheric cutoff at ~300 nm (see Figure 1; the atmospheric sky transmission decreases from ~16, 7, to 1.5% for wavelengths 310, 305 and 300 nm). Furthermore, the proposed spectrograph would be part of the VLT suite of instrumentation and as such needs to respect at some level bounds set by already existing or to be built capabilities. Most noteworthy in this context is the ESPRESSO spectrograph, which offers medium to high spectral resolution and throughput *redwards* of 380 nm (see Section 8.1). While some wavelength overlap is advisable (e.g. cross calibration) clear bounds have to be accepted. The science team felt that wavelength coverage beyond ~400 nm for the proposed spectrograph would provide an unfavourable cost to benefit ratio and that those science cases are well covered by ESPRESSO.

A more detailed analysis of the science cases shows that the blue edge limit of the wavelength range is mostly driven by the important Be case (Section 6.4) with the 313 nm line and perhaps the OH(0,0) line at 308.5 nm as water tracer for comets (Section 6.10). With the inclusion of a reasonable margin this translates into a requirement of 305 nm. There are also the unique lines of Bi I 302.46nm and Ge I 303.97nm which offer exciting possibilities (Section 6.2). Given that the natural atmospheric cut-off is so close, we argue that as a *strong* goal the wavelength coverage should be extended down to 300 nm.

The red edge of the required wavelength range is driven by a number of science cases including the surface-gravity determination from the Balmer decrement asking for coverage up to 400 nm (Section 6.8), the extragalactic science case for the AGN where the important [OII] 372.7nm and [Ne III] 386.8nm lines should be covered (Section 7.2), the strong CN emission line seen in comets at 388 nm and also the strong Ca II doublet at 393 and 397 nm seen in the ISM. The Quasar absorption line cases (Section 7.3) benefit generally and directly from larger wavelength coverage and as such provide a driver for maximizing the coverage without specific wavelengths.

Additionally, the high density of metal absorption lines in the UV always provides the opportunity to include more relevant lines – at the red edge these include Ba II 389.1, Pr II 396.4, Sm II 389.6, and Eu II 393, 397.1 nm (Section 6.2).

In summary the red edge of the wavelength range should at least cover the wavelength range up to 390 nm with a goal to extend it to ~400 nm.

Given that an increase in spectral resolution must be traded with lower throughput and less wavelength coverage at constant number of detector pixels, we determined for each science case the minimum needed resolution. Particularly for the stellar science case this questions was studied in detail (Section 6.4.5) yielding a minimum of R ~ 20,000 (at 320 nm) thus ensuring determination of Be and other important metal lines in the UV. Interestingly, a number of other science cases (perhaps most notably the Quasar absorption line cases; Section 7.3) ask for the provision of lower resolution modes within the same spectrograph. We argue that the spectrograph should (if technically feasible and affordable) include the provision for at least one lower spectral resolution option.

Summary:

- Required wavelength coverage: 305 – 390 nm (goal: 300 – 400 nm)
- Required spectral resolution: R = 20,000 – 22,000 at 320 nm with the addition of at least one more lower spectral resolution mode of R ~ 10,000 (or equivalent spacings for more modes)

9.3 Required S/N ratios and exposure times

Typical S/N ratios required for the science case run from about 10 (Section 7.3) to 50 (e.g. Sections 6 and 7.2) and to 100 and even 200 (Section 6.4). While the low S/N ratio science, often applied to faint targets, provides the typical demands for high throughput of the spectrograph, the high S/N cases set stringent requirements on the detailed system performance.

Faint targets and low sky fluxes in UV spectroscopy make the read-out-noise of the detector an interesting issue. In long (30-45min) exposures the noise should remain roughly sky limited at the bluest relevant wavelength (i.e. 315 nm) translating into a goal of RON <=2 e-/pix/DIT and a dark current rate of < 0.001 e-/pix/s (see Sections 6.4.5 and 7.3.5).

Several science cases, perhaps most prominently the stellar ones, demand high S/N ratios (~200). Here it is important that a detailed error budget is being constructed and the leading error sources identified in the next phase of the project. Items to investigate include, detector flat-field accuracy, detector point-spread-function, wavelength stability in relative and absolute terms, and spectrum extraction algorithms. Additionally, the calibration concept of spectrograph shall allow for obtaining high S/N spectra (S/N ~200) in one exposure, i.e. without the need for dithering along the slit and combination of multiple exposures.

For faint targets and/or high S/N ratios long exposure times are needed. Given the maximum observing block (OB) length of one hour this translates into about 45min exposure time. The stability of the spectrograph as well as the detector system (e.g. cosmic ray sensitivity) shall not be the limiting factor for such long exposures.

For the observations of extremely bright targets short exposure times are necessary. Using V=2 as a guideline for the maximum brightness an exposure time as short as 0.5 s needs to be enabled.

The science case as presented in this document largely focuses on observations of relatively faint targets (V > 13) and/or high S/N ratios. Therefore, even with the proposed, high efficiency

spectrograph the minimum **typical** exposure times are likely to be of order a few hundred seconds. For comparison the mean and median exposure times for optical X-shooter observations are ~340 and ~140 seconds with a strong peak at very short exposure times of a few seconds. The latter suggests that also for CUBES programs with bright objects yielding short exposure times will be executed.

Summary:

- For bright sources (e.g. V <10), the spectrograph shall be capable of delivering S/N ratios of up to 200 per spectral bin in one exposure.
- For faint targets and reasonably long exposures (30-45min) the noise contribution from the detector system should not exceed the one from the sky at wavelengths >315nm.
- The spectrograph (including the detector system) shall enable uninterrupted exposure times of up to at least 1 hour. The shortest exposure time shall be equal to or shorter than 0.5 s.
- The duty cycle of the spectrograph shall be targeted at a mean exposure time of 100 seconds and longer. It shall however also provide readout modes which allow for efficient observations of bright targets with short (e.g. 10 seconds) exposure times. This is also relevant for obtaining calibration data.

9.4 Pixel scale

For all science cases only seeing limited observations are envisaged and as such it seems advisable to set the pixel sampling appropriate to the median seeing conditions at ~350 nm which are of order 0.8”. The appropriate spatial sampling can be achieved with detector binning.

9.5 Targets and field-of-view

Typical targets for this spectrograph will be either point sources (stars) or only slightly extended objects. Several thousand potential targets are available for each of the stellar and extragalactic science cases. Even though the sky is relatively dark in the UV accurate sky subtraction is mandatory. Using X-shooter as a guideline, a 10” long slit seems appropriate.

Target magnitudes span a large range from potentially very bright comets (V~2) to very faint stars or QSO targets (V~21-22). It is therefore important that the acquisition system of the spectrograph can deal with a large range in target magnitude.

Summary:

- Slit length shall be at least 10”
- The acquisition of targets spanning V=2-22 shall be enabled.

9.6 Data reduction pipeline

For a modern spectrograph it is mandatory to provide a data reduction pipeline, which is capable of producing science ready products (see also VLT-SPE-ESO-19000-1618 “Data Flow for VLT/VLTI Instruments Deliverables Specification”). This includes the estimation of errors for the final data product. For many of the important science cases listed in this document it is necessary to combine several (long) exposures in order to achieve the final data-product. The pipeline should therefore foresee the capability to combine spectra from different observing blocks possibly executed during different nights.

References

Adelberger, K.L., Steidel, C.C., Shapley, A.E., Pettini, M., 2003, ApJ 584, 45

Andreani P., Ferlet R., Vidal-Madjar A., 1987, Nature, 326, 770

Antonucci, R. R. J. & Miller, J. S., 1985, ApJ, 297, 621

Antonucci, R., 1993, ARA&A, 31, 473

Arnould et al., 2007, Physics Reports, 450, 97

Baldwin, J. A., Ferland, G. J., Korista, K. T., Hamann, F., & LaCluyzé, A., 2004, ApJ, 615, 610

Barbuy et al. 2011, A&A, 534, A60

Blandford, M. D. & McKee, C. F., 1982, ApJ, 255, 419

Boesgaard, Tripicco, 1986, ApJ, 302, L49

Boesgaard et al., 2011, ApJ, 743, 140

Boroson, T. A. & Green, R. F., 1992, ApJS, 80, 109

Bowen I.S., 1934, PASP, 46, 146

Bowen I.S., 1935, ApJ, 81, 1

Bower, R.G., Benson, A.J., Malbon, R., Helly, J.C., Frenk, C.S., et al., 2006, MNRAS 370, 645

Cappetta, M., D'Odorico, V., Cristiani, S., Saitta, F., Viel, M., 2010, MNRAS 407, 1290

Cid Fernandes, R., Gu, Q., Melnick, J., Terlevich, E., Terlevich, R., Kunth, D., Rodrigues Lacerda, R., & Joguet, B., 2001, MNRAS, 355, 273

Cid Fernandes, R., González Delgado, R. M., Schmitt et al., 2004, ApJ, 605, 105

Coppolani, F., Petitjean, P., Stoehr, F., Rollinde, E., Pichon, C., et al., 2006, MNRAS 370, 1804

Cowan, J.J., Sneden, C., Beers, T.C., 2005, ApJ, 627, 238

De Avilez M. and Breitschwerdt D., 2005, A&A 436, 585

Debes J., et al, 2012, ApJ, 754, 59

Decressin et al., 2007, A&A, 464, 1029

Elvis, M., Wilkes, B. J., McDowell, J. C., Green, R. F., Bechtold, J., Willner, S. P., Oey, M. S., Polomski, E., & Cutri, R., 1994, ApJS, 95, 1

Farihi J., Jura M., Lee J., Zuckerman B. , 2010(a), ApJ 714(2), 1386

Farihi J., et al, 2010(b), MNRAS 404(4), 2123

Ferland, G. J., Hu, C., Wang, J.-M., Baldwin, J. A., Porter, R. L., Van Hoof, P. A. M., & Williams, R. J. R., 2009, ApJ, 707, L82

Gianninas et al., 2011, ApJ, 743, 138

Gilli, R., Vignali, C., Mignoli, M., Iwasawa, K., Comastri, A., & Zamorani, G., 2010, A&A, 519, 92

González Delgado, R. M., Heckman, T., & Leitherer, C., 2001, ApJ, 546, 845

Gratton et al., 2004, ARA&A, 42, 385

Haniff, C. A., Wilson, A. S. & Ward, M. J., 1988, ApJ, 334, 104

Heckman, T. M., 1980, A&A, 87, 152

Herald, J. E., Bianchi, L., 2004a, ApJ.609, 378

Herald, J. E., Bianchi, L., 2004b, ApJ.611, 294

Joly, M., 1987, A&A, 184, 33

Jura, M., Muno, M. P., Farihi, J., & Zuckerman, B., 2009, ApJ, 699, 1473

Kaiser M. and Wright L., 1990, ApJ 356, L1

Kerber et al., 2003, A&A, 408, 1029

Kewley, L. J., Groves, B., Kauffmann, G., & Heckman, T., 2006, MNRAS, 372, 961

Kilic M. et al, 2012, MNRAS 419 , L59

Kollmeier, J. A., Onken, C. A., Kochanek, C. S. et al., 2006, ApJ, 648, 128

Kratz, K.-L., Farouqi, K., Pfeiffer, B. et al., 2007, ApJ, 662, 39

Krugler, J.A., Boesgaard, A.M., 2008, ASPC, 393, 227

Lallement R., Welsh B.Y., Barstow M., Casewell S., A&A, 533, 140

Lebre et al., 1999, A&A, 345, 936

Linsky J, Rickett B., Redfield S., 2008, ApJ 675, 413

Liu X., Danziger J., & Murdin P., 1993, MNRAS, 262, 699.

McKee C. and Ostriker J., 1977, ApJ 218, 148

Melendez et al., 2009, ApJ, 704, L66

Milanova, Yu. V., Kholtygin, A. F., 2009, Astron. Lett. 35, 518

Miller Bertolami et al., 2006, A&A, 454, 845

Moy, E. & Rocca-Volmerange, B., 2002, A&A, 383, 46

Mullaney, J. R. & Ward, M. J., 2008, MNRAS, 385, 53

Napiwotzki & Rauch 1994, A&A, 285, 603

Nissen, P. E., & Schuster, W. J., 1997, A&A, 326, 751

Nissen, P. E., & Schuster, W. J., 2010, A&A, 511, L10

Noterdaeme, P., Ledoux, C., Petitjean, P., Srianand, R., 2008, A&A 481, 327

Noterdaeme, P., Petitjean, P., Srianand, R., Ledoux, C., \& López, S., 2011, A&A, 526, L7

Ogle, P. M., Cohen, M. H., Miller, J. S., Tran, H. D., Goodrich, R. W., & Martel A. R., 1999, ApJS, 125, 1

Osterbrock, D. E. & Dahari, O., 1983, ApJ, 273, 478

Pasquini et al., 1997, A&A, 325, 535

Pasquini, L., Bonifacio, P., Randich, S., Galli, D., & Gratton, R. G., 2004, A&A, 426, 651

Pasquini et al., 2005, A&A, 436, L57

Pasquini, L., Bonifacio, P., Randich, S., et al., 2007, A&A, 464, 601

Pasquini et al., 2008, A&A, 489, 315

Pogge, R. W., 1989, ApJ, 345, 730

Postman, M., arXiv:0904.0941; RFI submitted to Astro2010 Decadal Committee

Prantzos N., 2012, A&A 542, 67

Primas et al., 2000a, A&A, 364, L42

Primas et al., 2000b, A&A, 362, 666

Radovich, M., Hasinger, G. & Rafanelli, P., 1998, AN, 319, 325

Rafanelli, P., D'Abrusco, R., Ciroi, S., Cracco, V., Di Mille, F., & Vaona, L., 2009, NewAR, 53, 186

Redfield S. and Linsky J., 2008, ApJ 673, 283

Reeves et al.,1970, Nature, 226, 727

Rollinde, E., Srianand, R., Theuns, T., Petitjean, P., Chand, H., 2005, MNRAS 361, 1015

Scannapieco, E., Pichon, C., Aracil, B., Petitjean, P., Thacker, R.J., et al., 2006, MNRAS 365, 615

Schaye, J., Aguirre, A., Kim, T.-S., Theuns, T., Rauch, M., Sargent, W.L.W., 2003, ApJ 596, 768

Schmidt, G. D. & Hines, D. C., 1999, ApJ, 512, 125

Sestito, Randich, 2005, A&A, 442, 615

Smiljanic, R., Pasquini, L., Bonifacio, P., et al., 2009, A&A, 499, 103

Smiljanic et al. , 2010, A&A, 510, A50

Smiljanic et al. , 2011, A&A, 535, A75

Soderblom et al., 1993, AJ, 105, 2299

Solórzano-Iñarrea, C., Tadhunter, C. N., & Axon, D. J., 2001, MNRAS, 323, 965

Srianand, R., Noterdaeme, P., Ledoux, C., Petitjean, P., 2008, A&A 482, L39

Stanghellini, L., Shaw, R. A., Gilmore, D., 2005, ApJ. 622, 294

Suzuki, Yoshii, 2001, ApJ, 549, 303

Tan, Zhao, 2011, ApJ, 738, L33

Theuns, T., Leonard, A., Efstathiou, G., Pearce, F.R., Thomas, P.A., 1998, MNRAS 301, 478

Thielemann, F.-K., Hirschi, R., Liebendörfer, M., & Diehl, R., 2011, Lecture Notes in Physics, Berlin Springer Verlag, 812, 153

Vergely J.L., Valette B., Lallement R., Raimond S, 2010, A&A, 518, 31

Véron-Cetty, M.-P. & Véron, P., 2010, A&A, 518, 10

Veilleux, S. & Osterbrock, D. E., 1987, ApJS, 63, 295

Ventura, D'Antona, 2009, A&A, 499, 835

Vestergaard, M., 2002, ApJ, 571, 733

Vestergaard, M. & Peterson, B. M., 2006, ApJ, 641, 689

Wandel, A., Peterson, B. M., & Malkan, M. A., 1999, ApJ, 526, 579

Welsh B., Lallement R., Vergely J.-L., Raimond S., 2010, A&A 510, 54

Werner 1996, ApJ, 457, L39

Williams, R., Mason, E., Della Valle, M., & Ederoclite, A., 2008, ApJ, 685, 451

Wilson, A. S. & Tsvetanov, Z. I., 1994, AJ, 107, 1227

End of document